SEATANI: hazards from seamounts in SouthEast Asia, Taiwan, and Andaman and Nicobar Islands (eastern India)

Andrea Verolino[1], Su Fen Wee[2], Susanna F. Jenkins[1,2], Fidel Costa[1,2,3], Adam D. Switzer[1,2]

[1]Earth Observatory of Singapore, Nanyang Technological University, 50 Nanyang Ave, Singapore, 639798, Singapore

[2]Asian School of Environment, Nanyang Technological University, 50 Nanyang Ave, Singapore, 639798, Singapore

[3]Institut de Physique du Globe de Paris, Université Paris Cite, CNRS, 1 Rue Jussieu, Paris, 75005, France

Correspondence to: Andrea Verolino
Email: andrea.verolino@ntu.edu.sg

Abstract. Submarine volcanism makes up approximately 85% of volcanism taking place on Earth, and its eruptions have the potential to cause several hazards, including ash dispersal, pumice rafts, pyroclastic density currents, sector collapses and tsunamis. Recent examples include the eruptions in Japan and in the Kingdom of Tonga in 2021 and 2022 respectively, but there has been little to no study of submarine volcanism in Southeast Asia and its surroundings. Here we provide a compilation of 466 seamounts from the region, from different published sources, through the SEATANI dataset (Southeast Asia + Taiwan + Andaman & Nicobar Islands). We use this newly compiled dataset to assess on a regional level the seamount hazard potential and exposure potential as a springboard for future more quantitative hazard studies for the region. The hazard potential was assessed through seamount morphological/structural analyses, to determine the seamount evolution stage and, grade of maturity. The exposure potential was evaluated with two different approaches: An areal analysis of the number of assets within a 100 km radius of each seamount; and the development of a hazard-weighted seamount density map to highlight potential areas of interest for future more-in-depth studies. Our results show that there are several potentially hazardous seamounts in this region, and Taiwan had the highest hazard and exposure potential, for all assets considered, while Philippines, Indonesia and Vietnam have relatively high exposure potential for submarine communication cables and ship traffic density. The results from this work serve as a first step for Southeast Asian and neighbouring countries to become more resilient against and prepared for submarine volcanic eruptions in the region.

1 Introduction

Volcanic seamounts are submerged or mostly submerged volcanoes, and can be defined as "*any geographically isolated topographic feature on the seafloor taller than 100 m, including ones whose summit regions may temporarily emerge above sea level*" (Staudigel et al., 2010). The number of volcanic seamounts around the world is in the order of tens of thousands. A recent estimate suggests that there are ~35,000 seamounts >400-m in height (Gevorgian et al., 2023); however, limitations in detection suggest that this is a significant underestimate, especially in shallow continental shelf regions close to land masses (Kim and Wessel, 2011). Volcanic seamounts are generally detected through satellite-derived altimetry and gravimetry, however, these methods are limited by

resolution (i.e. kilometric scale, not allowing for the detection of small seamounts), and noise in the gravimetry measurements in areas with thick sequences of sediments (e.g. within continental margins; Kim and Wessel, 2011). It is likely that there are many more seamounts globally than those we are aware of.

Volcanic seamounts, particularly deep-sea ones, have been traditionally considered to be a negligible threat to society (Cas, 1992; Whelley et al., 2015), for several reasons. The first is that most of them are completely underwater, hence they are economically and logistically difficult to monitor, map and sample compared to their subaerial counterparts; as a result, their eruption frequency and intensity have not been properly assessed. A second reason is that they are often located far from major landmasses, hence not considered an imminent threat to populations. Thirdly, most of them have their summit in deep waters (> 3000 m b.s.l.), and this makes them hypothetically less hazardous than shallower volcanoes, because of the high hydrostatic pressure hindering explosivity. Finally, most ocean intraplate volcanoes, particularly those approaching subduction zones, are likely to be extinct and have not been active for millions of years (Staudigel and Clague, 2010), hence, have been not considered of interest for volcanic hazard. As a result, seamounts are vastly understudied around the world. In January 2022, the eruption of Hunga volcano in the SW Pacific (Kingdom of Tonga), demonstrated that erupting seamounts can have a large impact on people and their activities, even in a remote location such as the southwest Pacific Ocean. The eruption produced the highest volcanic plume ever recorded (~58 km) (Taha et al., 2022), unusually fast tsunamis that travelled across the Pacific Ocean for thousands of kilometres (Gusman et al., 2022), and damage of millions of USD across the entire region, with the Kingdom of Tonga being the most affected (damage equivalent to ~19% of the national GDP, and several casualties recorded) (The World Bank, 2022).

A few notable seamounts around the world have been studied in detail using multibeam surveys to obtain high resolution bathymetry (up to 1-m), and in a few cases were accompanied by sampling and/or video recording of the eruptions from Remotely Operated Vehicles (ROV's). Typically, these investigations occur after an impactful eruption. Examples include Havre volcano, (Kermadec arc), NW Rota-1 (Mariana arc), West Mata (Tonga arc), Fani Maoré (NW of Madagascar), Axial caldera (Juan de Fuca ridge) (Carey et al., 2014; Murch et al., 2019a; Dürig et al., 2020; Embley et al., 2006; Chadwick et al., 2008; Schnur et al., 2017; Clague et al., 2011; Dziak et al., 2015; Murch et al., 2022; Feuillet et al., 2021; Hammond, 1990; Caress et al., 2012; Clague et al., 2013). ~~(Carey et al., 2014; Murch et al., 2019a; Dürig et al., 2020(Embley et al., 2006; Chadwick et al., 2008; Schnur et al., 2017Clague et al., 2011; Dziak et al., 2015; Murch et al., 2022Hammond, 1990; Caress et al., 2012; Clague et al., 2013, in the Kermadec arc (north of New Zealand), which erupted in 2012 and produced what is considered one of the largest submarine silicic eruptions ever recorded (Carey et al., 2014; Murch et al., 2019a; Dürig et al., 2020); NW Rota-1 in the Mariana arc (Embley et al., 2006; Chadwick et al., 2008; Schnur et al., 2017), and West Mata in the Tonga arc (Clague et al., 2011; Dziak et al., 2015; Murch et al., 2022), which produced medium-intensity Strombolian explosions and lava flows (both eruptions were recorded); Fani Maoré volcano, offshore Mayotte island (NW of Madagascar), which was formed between 2018 and 2019, growing more than 800-m from the seafloor, and erupting both explosive and effusive products, despite being mostly basanitic in composition (Feuillet et al., 2021); Axial caldera, on the Juan de Fuca ridge (offshore of California, USA), which produced several effusive basaltic eruptions in recent years (last eruption in 2015), but also has evidence of past large explosive eruptions (Hammond, 1990; Caress et al., 2012; Clague et al., 2013),~~ among others. All the above-mentioned submarine volcanoes were surveyed as part of large, well-funded, multidisciplinary projects that provided a wealth of data (bathymetry, rock geochemistry, tephra granulometry and componentry, etc.). It is

logistically impossible to apply the same approaches to the thousands of seamounts worldwide, therefore, a regional approach is needed to characterise seamounts in a simple and efficient manner that allows for a broad focus on lesser-known areas potentially at risk.

Past global studies on volcanic seamounts have included classifications based on morphology or growth stage of the edifice (Schmidt et al., 2000; Wessel, 2007; Staudigel and Clague, 2010; Kim and Wessel, 2011; Gevorgian et al., 2023). Some authors found direct relationships between seamount morphometric parameters (e.g. basal width and height) and linked them to the tectonic setting (Schmidt et al., 2000; Gevorgian et al., 2023). These classifications, however, have never been used for assessing hazard potential or exposure on a regional scale.

For the region of Southeast Asia (SEA), there has been some effort in assessing hazards from what we define here as volcanic seamounts; examples include Krakatau and Banua Wuhu, Indonesia, and Didicas, Philippines (Hamzah et al., 2000; Paris et al., 2014; Mutaqin et al., 2019; Hidayat et al., 2020; Zorn et al., 2022; NCEI/WDS, n.d.), however, these studies focused on volcanic islands, and there is little or no consideration for the hazard potential from fully submerged volcanoes.

Our newly compiled dataset includes 466 seamounts from different sources (Fig. 1, Table S1 – Supplementary information) and enclosed within three (Indonesia, Philippines and Vietnam) of the nine Exclusive Economic Zones (EEZs) of Southeast Asia (Brunei, Burma, Cambodia, Indonesia, Malaysia , Philippines, Singapore, Thailand and Vietnam) and the neighbouring countries Taiwan and eastern India (Andaman and Nicobar Islands), and has been named SEATANI (**SEA** + **T**aiwan + **A**ndaman & **N**icobar **I**slands). This dataset includes both fully submerged volcanoes and some small volcanic islands, whose submerged portion makes up most of the edifice.

This region is interesting for several reasons: (i) It is very volcanologically active, but little is known about its underwater features; (ii) Millions of people live along its coasts; (iii) There are infrastructure worth billions of dollars on the seafloor of the target area (e.g. submarine telecommunication cables) (Wang et al., 2019); and (iv) It has a rather high density of ship traffic. Based on thisIn this paper, we have two main goals: one is to characterise the seamount morphology and evolution stage and link them to the *hazard potential* for seamounts in the region, and the other is to highlight areas of high *exposure potential*, to motivate and focus future studies. To accomplish the first goal of characterising seamounts and assess their hazard potential, we conduct qualitative (seamount type: caldera, guyot, simple cone, composite cone) and quantitative morphological analysis (height, summit water depth) by using open-access bathymetry datasets (e.g. Gebco 2021; NOAA DEM Global Mosaic; NOAA Multibeam Bathymetry Mosaic). Additionally, we also conducted a more qualitative analysis based on higher resolution bathymetry (Multibeam data from NOAA – 90m/pixel), where we highlight key seamount features (e.g. submarine landslides, explosive craters, new seamounts) that otherwise would not be detected from Gebco or the NOAA DEM Global mosaic dataset. Despite the multibeam data having limited regional coverage (< 10%), they reveal significant seafloor morphologies that can motivate future quantitative hazard assessments for the region, e.g. numerical hazard modelling. The second goal of highlighting areas of high exposure potential is achieved through two types of analysis, a quantitative one, where the number of assets and activities (population, submarine fibre-optic cables, and ship traffic density) within 100 km of volcanic seamounts is counted; and a semi-quantitative one, where the hazard potential of each seamount is used to weight the potential areal hazard extent for the entire region of interest. We acknowledge that our work has some limitations, in particular, the hazard and exposure potential are not quantified based on geological, geochemical, tectonic setting, age, and frequency/magnitude information, which are indeed needed for more quantitative studies (a focused discussion is

119 provided later in the text to address these points). However, our intent with this work is to provide the basic but

120 fundamental elements for future more quantitative studies.

2 Methods

2.1 Compilation of SEATANI

123 Following the seamount definition from Staudigel et al. (2010), here only used for volcanic seamounts, we pre-

124 compiled a list of seamounts for the region of interest by using three different types of sources: 1) The GVP

125 database (Global Volcanism Program 2013), where we include seamounts that have erupted from the Pleistocene

126 (n= 42); 2) The seamount dataset Gevorgian et al. (2023) (n= 405), which is an updated version of the dataset

127 from Kim and Wessel (2011), where they used statistical methods to differentiate volcanic from non-volcanic

128 seamounts; and 3) Seamounts from individual studies around the southeast Asian region found in literature (n=

129 35) (Li et al., 2013; Fan et al., 2017), which have been detected through geophysical methods (i.e. interpretation

130 of seismic profiles), for a total of 482 entries for the region considered. The definition proposed by Staudigel and

131 colleagues, however, does not provide specific directions on islands (at what extent a volcanic island is still

132 considered a seamount). Therefore, in order to guarantee reproducibility and to maintain our broad focus on the

133 unknown hazard potential of seamounts, we did not include islands whose emerged volume was > 30% of the

134 total seamount volume, and/or their maximum elevation was > 1000 m above sea level (a.s.l.) (more details on

135 this methodology are provided in the supplementary information). Following this criterion, none of the seamounts

136 from the Gevorgian et al. (2023) dataset or from the literature studies were removed, however, 16 GVP volcanoes

137 were excluded (Table S2, Supplementary information), bringing the total to 466 volcanic seamounts. Despite the

138 choice of 30% and 1000 m a.s.l. was somewhat arbitrary, it allows comparisons across studies and is in line with

139 our focus here, which is primarily on submarine volcanoes.

2.2 Bathymetry and exposure datasets

142 For the bathymetry, we used different datasets of different resolution based on each specific purpose. namely

143 These include *Gebco 2021*, *DEM global mosaic* (from NOAA/NCEI), and *Multibeam Bathymetry Mosaic* (from

144 NOAA/NCEI). Gebco 2021 is a gridded bathymetric dataset with interval grid of 15 arc-second (450-m/pixel),

145 and was used for the quantitative morphological classification (seamount growth stages) and exposure potential

146 analyses (quantitative and semi-quantitative). Despite the relatively low/medium resolution, it has global coverage

147 with bathymetry data deriving from different acquisition methods (Fig. S1, supplementary material), and was

148 clipped for the region of interest (North: 36.5°, South: -14.3°, West: 82.0°, East: 145.6°). The DEM global mosaic

149 is a colour shaded relief raster file that was exclusively used for the qualitative morphological classification

150 (seamount morphotypes); it is a seamless bathymetry/topography mosaic that combines DEMs from several

151 sources (e.g. direct and indirect measurements from ships and satellites) and different resolutions (450-m/pixel or

152 better), with the higher-resolution DEMs displayed on top of the lower resolution ones (where both available).

153 Since DEMs of different resolution cannot be extrapolated from this file, but must be downloaded individually,

154 we used the mosaic format for efficiency and for visualization purposes only. The file was clipped with the same

155 extent as Gebco 2021, for consistency. The Multibeam Bathymetry Mosaic is the dataset with the highest

156 resolution among the datasets used here (90-m/pixel); it is a gridded colour shaded relief, deriving from multibeam

157 survey data collected over the years (from ~1980 to present). This dataset has a coverage lower than 10% for the

158 region of interest, therefore was only used for qualitative image analyses, both for the morphological classification

4

159 (in combination with the DEM Global mosaic) and for the characterization of bathymetric features (see
160 discussion) at some of the locations enclosed within our study area (where there was data coverage).

161

162 To assess the exposure potential, we used different open-access datasets for population, submarine
163 communication cables and ship traffic density. We chose these assets for three reasons: (i) Data were available
164 for quantitative analyses on GIS environment on a regional scale; (ii) We considered them as the assets potentially
165 more exposed to multiple hazards from a submarine volcanic eruption in a regional perspective (e.g. air traffic
166 exposure was not quantified here because potentially only exposed to development of a tephra column); And (iii)
167 such exposure assessment from submarine volcanic eruptions has not been done before, particularly for submarine
168 communication cables and ship traffic density, which instead have shown to be vulnerable elements to natural
169 hazards (Ohno et al., 2022; Speidel, 2022). For population estimates, we used LandScan (Sims et al., 2022), which
170 has a spatial resolution of around 1 km (30 arc-seconds) and has been widely used in previous volcanic hazard
171 assessments (Reyes-Hardy et al., 2021; Jenkins et al., 2022; Verolino et al., 2022a). For the submarine cables we
172 used data from *TeleGeography* (last update in 2017); while for the ship traffic density we utilised data from *The*
173 *World Bank Group*, which reports hourly Automatic Identification Systems (AIS) positions, recorded between
174 January 2015 and February 2021, at a spatial resolution of 500-m/pixel. This dataset included separate files for
175 commercial, leisure, passenger, oil and gas, and fishing vessels respectively, however, we used the combined file,
176 assuming no distinction across vessel types.

177

178 **2.3 Volcanic seamounts classification**
179 Volcanic seamounts were classified through two different approaches: 1) Qualitative, based on seamount shape
180 (i.e. caldera, guyot, simple cone, composite edifice; Fig. 2 and Table 2); and 2) Quantitative, based on the
181 seamount height and depth that gives a stage of growth, as proposed by Staudigel and Clague (2010) (Stage 1 to
182 5: defined in Table 3). Both classifications were obtained from analyses conducted in GIS environment (Esri®
183 ArcMap 10.7.1). For the qualitative classification, we overlaid the seamount locations over the bathymetry
184 datasets, and conducted visual image analysis to establish morphotype (Table 2, Fig. 2), using the highest
185 resolution available for that area (NOAA DEM Global Mosaic, 450-m resolution or better, or NOAA Multibeam
186 data, 90-m resolution). This morphological assessment was conducted by authors A. Verolino and S.F. Wee, to
187 ~~verify~~ test for consistency and reproducibility, as the classification can be partially subjective. For the quantitative
188 method, we applied the Staudigel and Clague (2010) classification (used here for the first time for hazard
189 purposes) and obtained the seamount maximum summit height and base water depth within a 30 x 30 km bounding
190 box of the given seamount location (following Kim and Wessel, 2011). These were in turn used to assign a stage
191 of growth. Staudigel and Clague (2010) also included Stage 6 seamounts (those approaching the trench of a
192 subduction zone, or that already started being subducted), however, to maintain the growth stage classification in
193 a state that is as quantitative as possible, we included them within the low hazard potential i.e. Stage 1, 2 or 5
194 seamounts (i.e. deep-water or extinct seamounts). We did this depending on their height and water depth though
195 we know that the Staudigel and Clague (2010) classification, is not specific on how close to the subduction trench
196 a seamount must be to be considered stage 6, leaving some subjectivity in the classification). We used both
197 qualitative and quantitative classification approaches in parallel to obtain different types of information
198 (morphological and growth stage); however, for exposure calculation we refer only to the quantitative approach
199 (i.e. growth stage).

2.4 Exposure analysis

We conducted two types of exposure potential assessments: 1) A quantitative analysis of population, submarine communication cables and ship traffic density within 100 km from each seamount; and 2) A semi-quantitative assessment, through a hazard-weighted seamount density map, to assess what countries are more likely to be threatened by a seamount within the study region.

For the first type of assessment, we chose concentric 100 km radii to include exposure potential of the above-mentioned assets with the approximation that this would include the more damaging processes from most volcanic hazards (e.g. tephra fallout, PDCs, sector collapses). This choice is in line with previous regional volcanic threat studies (Small and Naumann, 2001; Brown et al., 2015), however, we acknowledge that using concentric radii is an oversimplification of volcanic hazard extents (Jenkins et al., 2022).

The semi-quantitative assessment considered the concentration of seamounts, weighted by their hazard rank (Table 1), and highlights regions of higher hazard potential. We created a weighted seamount density map (Kernel Density Estimation, KDE), based on the seamount stage of growth, with the assumption that more heavily weighted seamounts have a greater hazard potential. The KDE was performed on Esri® ArcMap 10.7.1, which assigns a default bandwidth in function of the input dataset (~630 km in this case), and proven to be reliable in previous exposure studies (Verolino et al., 2022a). To verify whether the default bandwidth was suitable to our case, we conducted additional KDEs by manually assigning different bandwidths (named "search radius" in ArcMap) in the range 800-100 km respectively; the results, reported in the supplementary material (Fig. S2), support our choice to use the default bandwidth. The choice of weight assigned to each growth stage (Table 1) was based on the Global Historical Tsunami Database (NCEI/WDS), where out of 164 historical volcanic tsunamis (from 1610 BC to present), 115 were from volcanic seamounts; of these, 78% (n= 90) were from stage 4, 20% (n= 23) from stage 3, and nearly 2% (n= 2) from stage 1, 2, 3 or 5 seamounts (depth of seamount unknown). To compensate the paucity of historical information/data from stages 3, 2, 1 and 5 (shallow or deep), compared to stage 4 seamounts (partially emerged), and to include volcanic hazards as well, we arbitrarily adjusted these percentages to 60% and 35% for stage 4 and stage 3 respectively, and the rest was distributed through stage 1, 2 and 5 seamounts (Table 1). Exposure potential was then assessed based on the extent of high-density area (higher exposure potential: $> 2.9 \times 10^{-6}$ seamounts/km^2) obtained from the KDE.

Table 1. Seamount hazard ranking based on the Global Historical Tsunami Database (NCEI/WDS) and growth stage from Staudigel and Clague (2010).

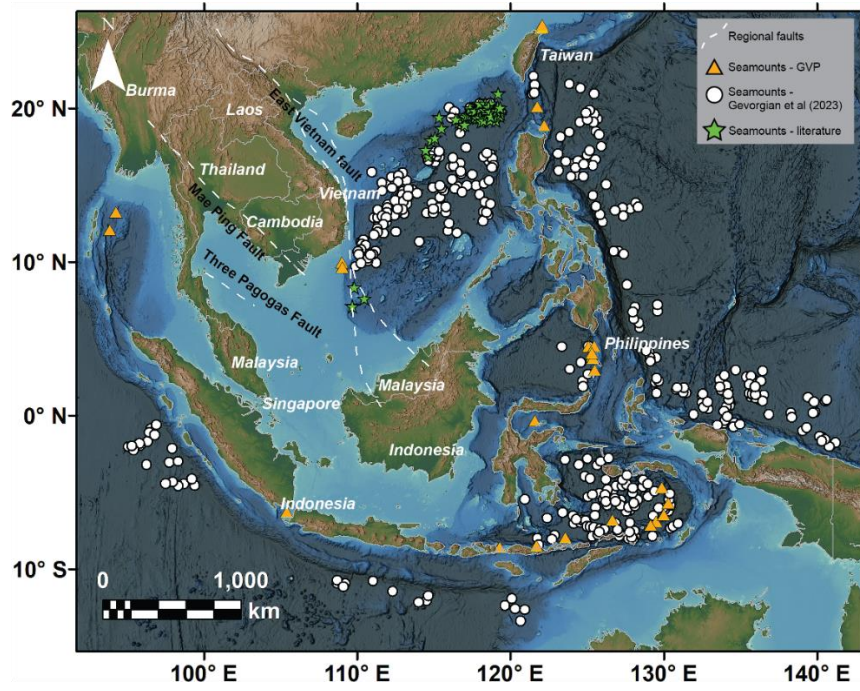| Seamount hazard ranking	Seamount growth stage	Historical volcanic tsunami occurrence (%)	Hazard weight
1	4	78	0.6
2	3	20	0.35
3	2		0.03
4	1	2	0.01
5	5		0.01

234 **Figure 1. Map of the study area with seamounts locations and major regional faults.**
235 **Basemap is from NOAA (DEM Global Mosaic).**

3 Linking seamounts morphology and evolution stage with their potential hazards

3.1 Seamount morphotype

238 Seamount morphology can be used to infer information about the seamount eruptive history. An important
239 consideration is that once seamounts are completely submerged, they do not experience major erosion, retaining
240 most of their original morphological constructive features, unless new eruptions and/or disruptive events such as
241 landslides take place. Therefore, classifying seamounts based on their large-scale morphological features
242 overcomes the resolution issue that we generally have at smaller scales. Below in Table 2 (examples shown in
243 Fig. 2), we provide general guidelines we used for the classification of seamount morphotypes. A background for
244 each morphotype, with a link to their hazard potential and with relevant examples from the literature, is provided
245 in the supplementary information file.

247 **Table 2. Seamount morphotype descriptions.**

Seamount morphotype	Description
Simple Cone	Regular-shaped and conical pointy volcanic edifice with only one vent
Composite edifice	Irregularly shaped volcanic edifice with one or more vents. This morphotype also includes ridges and flank ephemeral cones (e.g. subaqueous portion of a volcanic island)
Caldera	Volcanic edifice with prominent central depression with diameter ~ 4-8 km
Guyot	Flat-topped volcanic edifice with relatively steep flanks

3.2 Seamount growth stage

250 Staudigel and Clague (2010) classified seamounts based on their growth stage (Stage 1 to 5), here we use the same
251 approach to first assign a growth stage to the SEATANI seamounts, and then link the growth stage to a given
252 potential hazard(s) that may be common for that particular growth stage. In Table 3 we report the main

characteristics for each growth stage (from Staudigel and Clague, 2010), and associated potential hazards (Murch et al., 2019a; Paris et al., 2014; Clague et al., 1990; Harders et al., 2014; Verolino et al., 2018, 2019, 2022b; Jutzeler et al., 2014; Deardorff et al., 2011; Omira et al., 2016; Newland et al., 2022). A more comprehensive analysis of seamount growth stages and their potential hazards is provided in the supplementary information file.

Table 3. Seamount growth stage and associated potential hazards. Adapted from Staudigel and Clague (2010).

Seamount growth stage	Description (from Staudigel and Clague, 2010))	Potential hazards (see references in the text)
1	• Seamounts 100-1000 m high and > 700 m below sea level (b.s.l.) • > 80% lavas and < 20% pyroclastic deposits	• Lava flows • Obstacles for navigation (submarines)
2	• Seamounts > 1000 m high and > 700 m b.s.l. • > 80% lavas and < 20% pyroclastic deposits • Developed shallow magma plumbing system (especially the larger ones), potentially leading to flank instability	• Lava flows • Subaqueous eruption-fed density currents • Subaqueous eruption column • Pumice rafts • Large gas bubbles • Sector collapse • Tsunamis • Obstacles for navigation (submarines)
3	• Seamounts < 700 m b.s.l. • > 60% pyroclastic deposits • +/- Developed shallow plumbing system (depending on seamount size) • Higher flank instability due to abundance of pyroclastic material making up the seamount	• Lava flows • Subaqueous eruption-fed density currents • Subaerial PDCs • Subaqueous and subaerial eruption column • Pumice rafts • Sector collapse • Tsunamis • Obstacles for navigation (submarines)
4	• Emerged seamounts (> 70 vol% submerged) • > 60% pyroclastic deposits • +/- Developed shallow plumbing system (depending on seamount size) • High flank instability due to abundance of pyroclastic material making up the seamount	• Lava flows • Subaqueous eruption-fed density currents • Subaerial PDCs • Subaerial eruption column • Sector collapse • Tsunamis
5	• Flat-topped seamounts (guyots) • Originally emerged seamounts drowned below sea level for erosion and subsidence, and cessation of volcanic activity	• Obstacles for navigation (submarines)

4 Results

4.1 Seamount morphology and growth stage

Seamounts in our study were classified based on their morphotype (simple cone, composite edifice, caldera, guyot; Fig. 2, Table 2) and growth stage (Stage 1 to stage 5; Table 3). Results for their abundance, distribution and exposure analyses are reported below (Figs. 3-6).
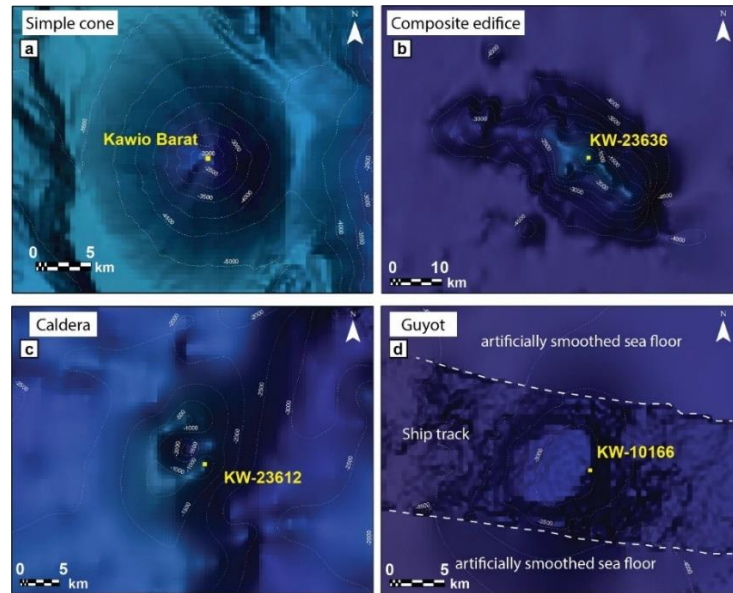

Figure 2. Seamount morphotype examples. Note how the seafloor appears smoothed away from ship track measurements due to low density of data points (d). The basemap shown here is from NOAA (DEM Global Mosaic).

Of the 466 seamounts in our catalogue, we were able to classify 295 (63%) of them into the four morphotypes; the remaining 171 (37%) seamounts were not classifiable due to low resolution bathymetry data and/or because they were too small. The seamounts are dominated by *composite* edifices (n= 255, 54.7%), followed by *simple cones* (n= 29, 6.2%), and guyots (n= 7, 1.5%). The morphotype least represented is calderas, with only 4 of them (0.9%). Water depths range from -5739 m b.s.l. (seamount KW-22106 of unknown morphotype; Lat: 13.81°, Lon: 125.58°) to 776 m a.s.l. (Paluweh, simple cone; Lat: -8.32°, Lon: 121.71°), with a *mode* of 2306 m b.s.l., *mean* -2106 m b.s.l., *median* -2221, and *skewness*= 0.02 (close to symmetric distribution) (Fig. 3c). Water depths within each morphotype category are relatively variable (Fig. 3d). Simple cones, composite edifices and calderas have a median of about 2000 m b.s.l., while guyots are mostly closer to sea level (median ~500 m b.s.l.), and unclassified seamounts cover the entire underwater range (~ 0-5700 m b.s.l.). Despite having a general broad range of water depths, all the classified seamounts are also represented at relatively shallow water depths (shallower than 1000 m b.s.l.), and this has important implications in terms of volcanic hazard (discussed in later sections). We found no particular geographic or tectonic setting distribution associated with each morphotype (Fig. 3a).

Results from the growth stage analysis (Fig. 3e) show that the majority of the seamounts in the study region are in their *stage 2* (65%, n= 303), > 1000 m high and > 700 m b.s.l., followed by the shorter but still deep *stage 1* (14%, n= 67), shallower *stage 3* (12%, n= 58), and emerged *stage 4* (7%, n= 31) seamounts. Only 7 seamounts (2%) represent *stage 5, flat-topped seamounts*. When comparing morphotype and growth stage distributions (Fig. 3f), simple cones and composite edifices are found in all growth stages, except for stage 5 (by definition), with composite edifices dominating across all stages. Calderas are only found within stage 2 (1%) and stage 3 (2%)

seamounts, however, when a caldera complex has new cones formed within them or on their rims, we classified them as composite edifices (e.g. Krakatau, Indonesia). Undefined seamounts dominate stage 1, however, they decrease in percentage towards higher stages seamounts. In terms of geographic/tectonic setting, stage 1 and 2 seamounts dominate extensional and/or intraplate domains such as back-arc basins (e.g. Banda Sea), and zones undergoing subduction (e.g. west of the Sumatra and Java trenches; east of the Philippines trench); while stage 3 and 4 seamounts are more common along volcanic arcs (e.g. Banda arc) and intraplate settings (Sunda Shelf, east of Vietnam; Fig. 1). An exception is represented by the South China Sea, an intraplate extensional setting, where the distribution of all grow stage seamounts is rather uniform, suggesting a more complex interplay of geological processes shaping seamount development.
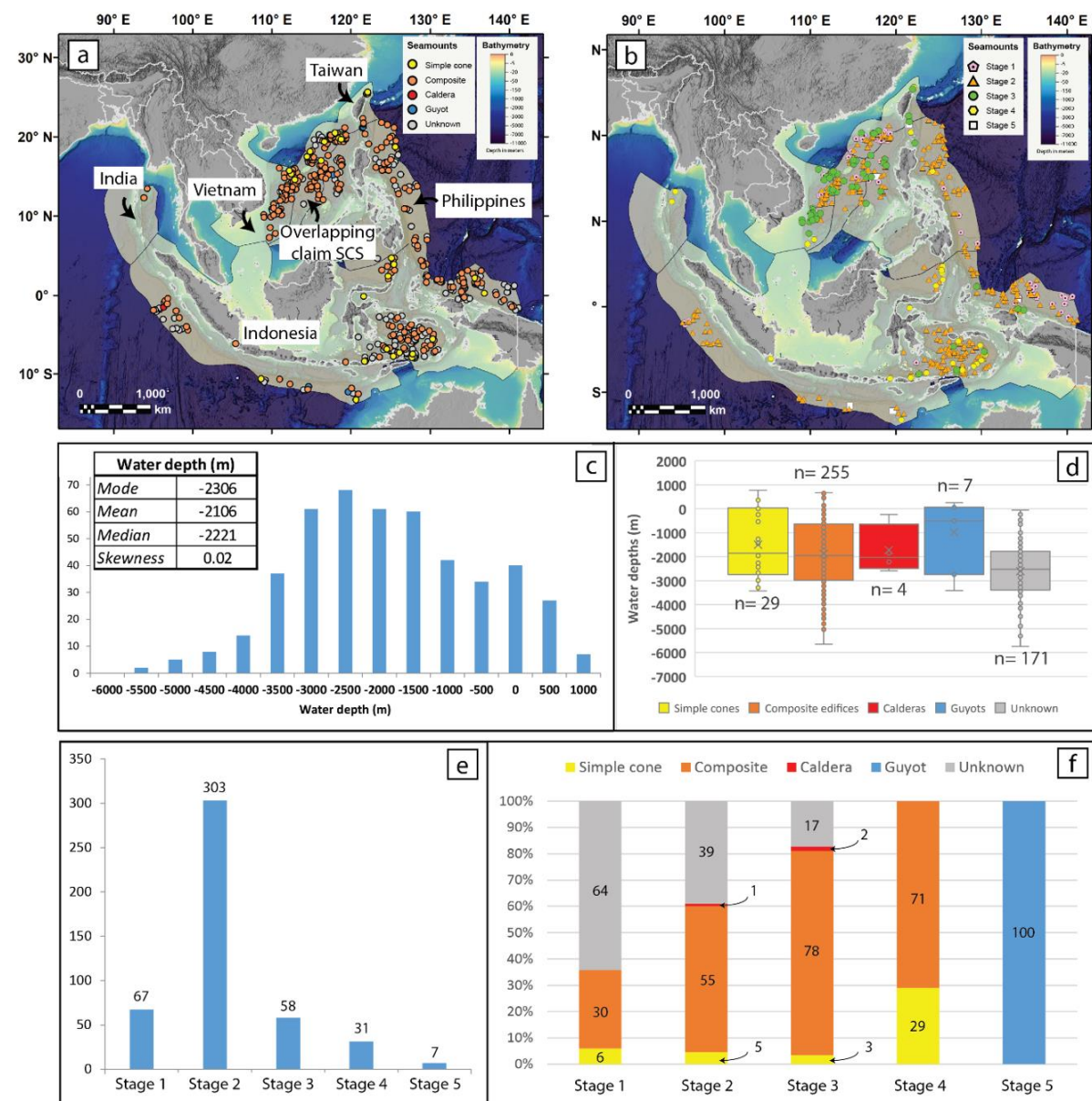
Figure 3. Results of seamount classifications. Seamounts distribution maps based on their morphotype (a) and growth stage (b) (basemap is from NOAA - DEM Global Mosaic; yellow polygons represent exclusive economic zones). Distribution plots of water depths (c), and water depths vs morphotypes (d). Distribution of seamount growth stages (e), and normalised distribution (%) of seamount morphotypes within each growth stage (f).
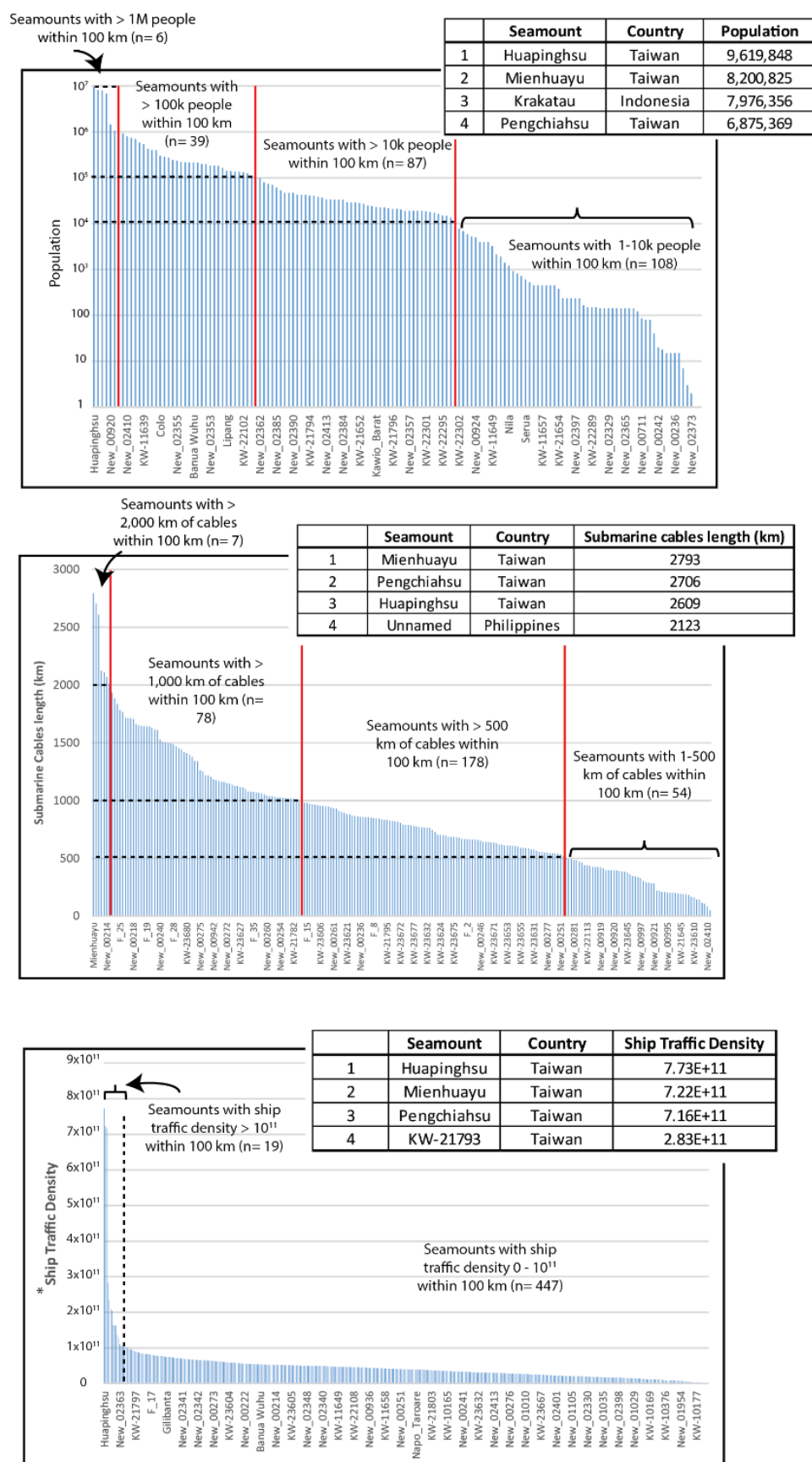
4.2 Analysis of 'Exposure Potential'

4.2.1 Exposure Potential of assets around seamounts (quantitative)

In this section we assess the exposure potential for population, submarine communication cables and ship traffic within 100 km radius from each seamount (Figures 4 and 5; Fig. S23 and Table S1). We found that 1.3% of the volcanoes of our catalogue (n= 6) have more than 1M people living within 100 km from them, with Huapinghsu (about 40 km north of Taiwan) exposing about 9.6M people, and two nearby volcanoes (Mienhuayu and Pengchiahsu) having a similarly high level of exposure (8.2M and 6.8M people), with Taipei lying approximately 60 km away. Krakatau volcano, Indonesia, also ranks high, with nearly 8M people exposed (Fig. 4, Fig. S23), many in Jakarta, which lies ~140 km to the east. About 8% (n= 39) of the seamounts expose between 100k and 1M people, and these are mostly located within the EEZs of Taiwan, Philippines and Indonesia. There are also a significant number of seamounts (n= 319) with zero population exposure, mostly located in the central portion of the northern South China Sea, western Pacific Ocean, and eastern Indian Ocean, and some in the Banda Sea.

Exposure for submarine cables has been evaluated in terms of total length of cables within 100 km from each seamount. About 50% (n= 232) of the seamounts have at least 50 km of submarine cables within their radii, and approximately 17% of seamounts (n= 78) expose more than 1000 km of cables each. The seamounts with higher exposure are within the EEZs of Taiwan, Philippines and Vietnam, with Taiwanese volcanoes exposing more than 2500 km of cables each (Fig. 4, Fig. S23).

Ship traffic density also shows the highest values around Taiwanese seamounts (Fig. 4, Fig. S23), with the busiest areas including the Taiwanese strait, western and eastern portions of the northern South China Sea (east of Vietnam and west of Philippines), Singapore and Malacca Straits, and Gulf of Thailand, with the last three having zero exposure due to lack of known seamounts nearby. Krakatau also ranks high for ship traffic exposure (11th).

In Figure 5, we aggregated exposure to the country level for individual seamount growth stages, and we found that 5 of the 11 EEZs in the region lie within 100 km of a volcanic seamount (India, Indonesia, Philippines, Taiwan and Vietnam), in addition to the central portion of the northern South China Sea, which is contended across different nations (i.e. here referred to as *overlapping claim waters*) and not discussed here. For population, Taiwan has the highest exposure values (up to nearly 10M people), followed by Indonesia (up to 8M) and the Philippines (< 1M). For exposure of submarine cables, Taiwan and the Philippines rank the highest (up to >2,000 km of cables nearby seamounts), followed by Vietnam, and the other EEZs having similar values, with overall less than ~1,500 km of cables within their maritime boarders. For ship traffic density, again, Taiwan reports the highest exposure, followed by the Philippines, Indonesia, Vietnam and India, with similar values respectively. When considering the growth stage, besides being the country with the highest exposure values, Taiwan is also the country with exposure to the seamounts with higher rank (stage 3 and stage 4), and this is shown for all the assets considered.

Figure 4. Exposure potential for population (top panel), submarine communication cables (middle panel) and ship traffic density (bottom panel) within 100 km from seamounts in and around SEA. Tables with the top 4 seamounts for exposure are also reported (full seamounts exposure lists are available as additional material; Table S1).
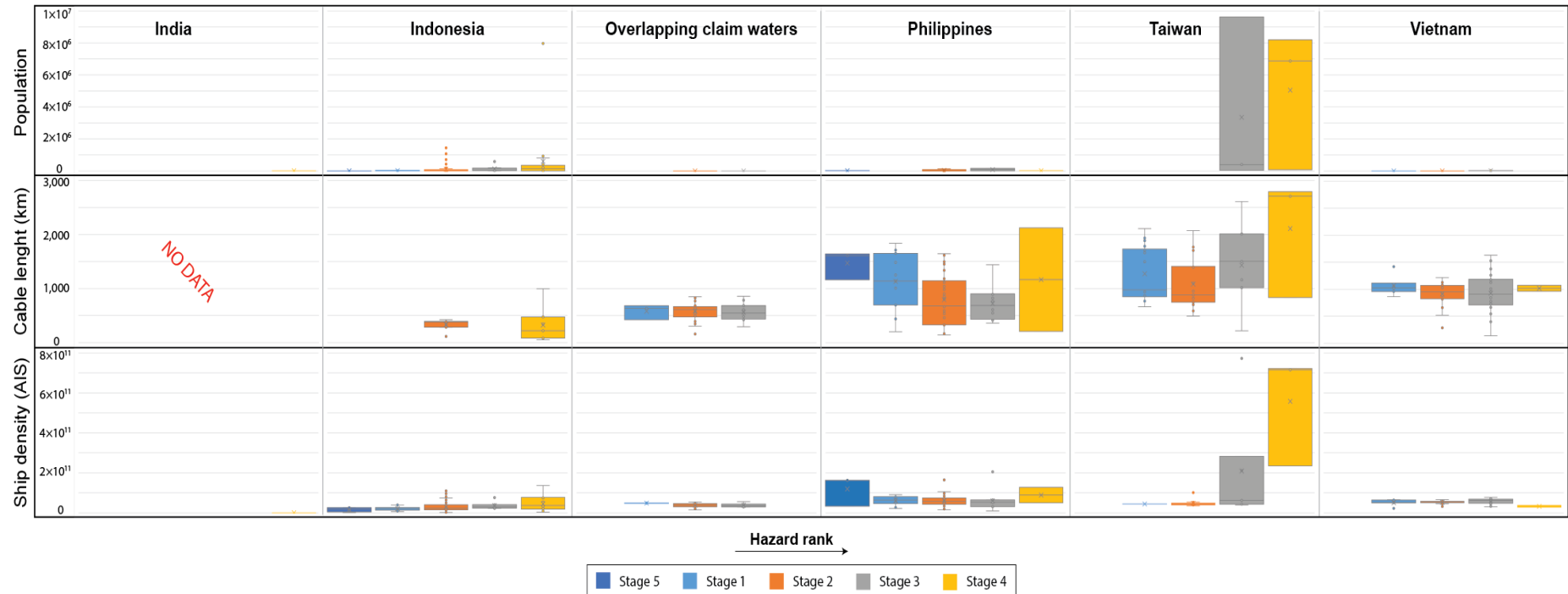
343
344 **Figure 5. Exposure potential by country across all stages (ordered from left to right with increasing hazard rank), for population, submarine cables, and ship traffic density. Note that**
345 **there is no cable data for India's seamounts**

4.2.2. Hazard weighted seamount density (semi-quantitative)

We conducted a weighted Kernel Density Estimation (KDE) to understand which regions have higher potential to produce hazards from a seamount. This estimation is purposely weighted towards the more hazardous seamounts (Stage 3 and 4) (more details about the weighting process are reported in the methods section). A sensitivity analysis was run with only stage 3 and 4 seamounts to test the effect of the lower-weighted stage 1, 2 and 5 seamounts, which represent the majority of the seamounts in our study, on the final weighted density map. Their effect was found to be minor (Fig. S4, Supplementary material), therefore we proceeded with this approach by including all seamount stages with a given hazard weight (Table 1). The results (Fig. 6) show that there are two large regions of interest, the largest is in the South China Sea, followed by the Banda Sea. Other areas of interest, but with lower density, include the Celebes Sea, the Halmahera Sea, and the portion of Pacific Ocean just east of Taiwan and northern Philippines. Countries surrounding the areas with higher weighted density include southern Vietnam, southern and northern Philippines, and eastern Indonesia (Sulawesi, Maluku, and Lesser Sunda Islands).
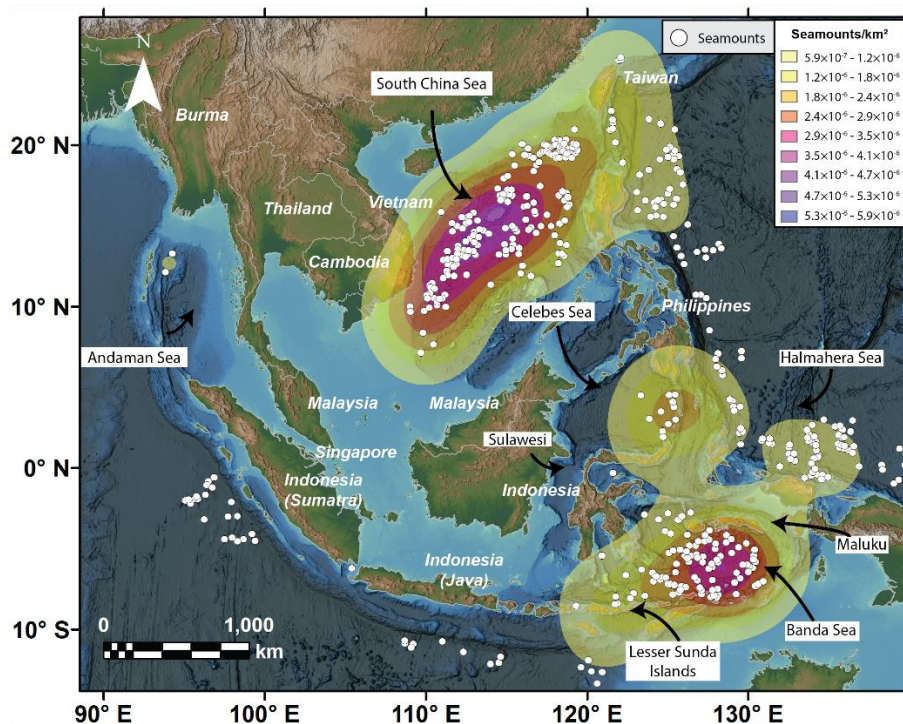

Figure 6. Hazard-weighted seamount density map in the region of interest. In dark purple the area with higher density of seamounts of higher hazard (see Table 1 for hazard weight).

5 Discussion

5.1 Potential sources of volcanic and related hazards in Southeast Asia and its surroundings

Our morphological assessment, while not incorporating geological, absolute age, and frequency/magnitude data (as further discussed in subsequent sections), offers valuable preliminary insights into the historical and possible future activities of seamounts. This approach is instrumental in identifying potentially hazardous seamounts for more detailed investigation in future research, as discussed below.

Mienhuayu and Pengchiahsu (offshore north of Taiwan), are two stage 4 simple cones, which lie in waters shallower than 200 m, with their summits just above sea level (16 and 49 m a.s.l. respectively). We can hypothesise that simple cones found in shallow waters in our region of interest are likely relatively young, because the sea

14

level rose about 120 m over the last ~20k years (Diekmann et al., 2008; Hanebuth et al., 2011). If volcanoes that are now in shallow water environments were already existing 20k ago, we could assume that they were at least partially above water, and this would be reflected in their shape (e.g. presence of prominent terraces on the flanks). Mienhuayu and Pengchiahsu, which have their base at ~200 m b.s.l., and are considered Pleistocene in Age (100 ka or younger: Global Volcanism Program 2013), would be good case studies to test this hypothesis, however, the current available resolution prevents us from providing reliable inferences at this stage. Focused bathymetric and/or seismic surveys around these volcanoes would provide key clues about their relative age (older or younger than the last glacial maximum, 25 ka). This is important for hazard assessment, because Mienhuayu and Pengchiahsu are 50-60 km of the Taiwanese mainland and are among the volcanoes that rank the highest in the quantitative exposure potential analysis for all the assets considered (Fig. 4) (more discussion in the following sections).

The Kawio Barat seamount (~100 km south of the Philippines; Lat: 4.68°, Long: 125.09°) is a large simple cone rising from about 5,500 m b.s.l. up to ~2000 m b.s.l. (stage 2); it is unlikely that such a high seamount was formed in a single or short-lived eruptive event. Its regular conical shape, its height and the relatively steep slope angles (up to >30°) suggest a past explosive or mixed explosive/effusive history, as observed at similar cones on land; therefore, it represents another candidate to attention for future studies.

In this study Krakatau has been classified as a composite and stage 4 seamount, even though it is the newest cone formed as part of a caldera complex. It is well known for the 2018 eruption collapse-tsunami event (Self, 1992), and for the catastrophic eruption of its predecessor in 1883, which produced PDCs and tsunamis, killing over 30,000 people (Self, 1992). An example of a less known but still potentially hazardous composite and stage 4 seamount in the region is North Kawio, Indonesia (northern portion of the Sangihe volcanic arc; Lat: 4.68°, Long: 125.47°). This seamount is reported as Pleistocene in the GVP, but no other information about age is provided. It is a mostly submerged edifice, with multiple peaks above sea level (e.g. Marore, Kawio, and Kamboreng islands) and several submarine vents, covering a total area of about 1,500 km². These characteristics (distributed volcanism), besides the unknown and possibly relatively young age, and the relatively close proximity to mainland southern Philippines (~100 km south), make North Kawio a potential seamount that could create tephra and tsunami hazards.

In terms of potentially more explosive submarine eruptions, calderas are key morphotypes to consider for the region. In our classification we identified 4 calderas, 3 of which have their summit at a water depth larger than ~1,300 m, with 2 of them being deeper than 2,000 m (all stage 2). Some calderas may form due to gradual subsidence over a longer period of time, hence not associated with any catastrophic explosive event. One key morphological indicator of either sudden or gradual collapse may be hidden in the intra-caldera slope angles; steep inner flanks may indicate a sudden sub-vertical movement downward resulting from the magma withdrawal from a shallow magma chamber. Despite the long-believed concept that explosive volcanic activity is hindered at large water depths (Cas, 1992), we show in our study that deep calderas with explosive features do exist. Seamount KW-23612, in the northern South China Sea (Fig. 2c), for example, despite having its rims reaching about 230 m b.s.l. (stage 3), has the caldera floor at over 2,000 m b.s.l., with inner slope angles up to ~50°. It is unlikely that such a depression (nearly 2,000 m deep), with such steep caldera walls was formed by gradual subsidence. Similarly, the recent eruption at the Hunga volcano, was responsible for deepening its caldera floor from an initial depth of about 200 m to about 850 m (Ribo et al., 2023). The eruption, although initiated at shallow water depth,

was responsible for the withdrawal of intra-caldera material up to >800 m through explosive mechanisms, and this has important implications, once again, about the water depth limit of volcanic explosive eruptions. It is clear that explosive activity associated with caldera formation can be of rather large magnitude, resulting in high hazardous scenarios, particularly if this occurs in highly populated areas such as the South China Sea (e.g. seamounts KW-23612, New-00258) or off the coasts of Indonesia (seamount KW-10401).

5.13.1 The geodynamic context for SEATANI seamounts

We noted that the geology, absolute age, and eruption frequency/magnitude, were not considered for our hazard-exposure potential assessment, because of the lack of information for most of the seamounts in the region. Notwithstanding, in this section we discuss the geodynamic context of the SEATANI seamounts from a regional perspective, with a particular focus on the two regions that we found to host the highest number of stage 3 and 4, hence potentially more hazardous, seamounts: the South China Sea and the Banda Sea.

There are aA number of seamounts (Fig. 6) in proximityclose to the Indonesian and Philippines trenches that show zero to very low weighted density, and this reflects their relatively low hazard potential. Seamounts in these particular tectonic settings are likely millions of years old and no longer active, being at the end of their cycle and approaching a subduction zone (Staudigel and Clague, 2010). It is likely that also some seamounts in the high weighted density regions of the South China Sea and Banda Sea may have been extinct for millions of years, however, these areas represent differentare in tectonic settings, and must be discussed separately.

The South China Sea is the result of a multiphase continental rifting and breakup from the Eocene to the Miocene (e.g. Franke, 2013). Many studies provide evidence for extensive intraplate volcanism in the South China Sea following the end of the continental rifting (e.g. Xia et al., 2018; Gao et al., 2019; Zhao et al., 2020), with abundance of Late Cenozoic OIB-type basalts, inferred to be linked to a mantle plume (Yang et al., 2019). A more recent study identified widespread and partially still ongoing hydrothermal activity in the northern South China Sea, thought to be associated with magma intrusion (Zhao et al., 2021). On the southwestern edge of the South China Sea, east of southern Vietnam, there is a submarine volcano that erupted in historical times, Ile des Cendres, 1923. The volcano is located in proximity to a major regional fault, the East Vietnam Fault (Hall and Morley, 2004; Li et al., 2013) (Fig. 1); other major faults exist in the region, Mae Ping Fault and Three Pagogas Fault (Hall and Morley, 2004; Li et al., 2013), Fig. 1), and others may not be mapped, together with volcanoes in their proximity. Therefore, despite the intraplate setting, volcanism in the South China Sea may still play a role for future hazardous scenarios for the region.

The Banda Sea, on the other hand, results from more complex geodynamics. This area was formed by the initial collision between the Australian and the Banda arc (which was already active from ~12 Ma, (Yang et al., 2021), and subsequent slab rollback, which created the extensional Banda Sea back-arc basin (Wei et al., 2023). Therefore, seamounts in this area belong to at least two different formation mechanisms, arc volcanism and back-arc extensional volcanism. If we consider the seamount growth stage for this area (Fig. 3b), we notice that that majority of seamounts along the Banda arc are stage 3 and 4, while the seamounts in the central portion of the Banda Sea basin are stage 2. Most of these stage 2 seamounts are likely as old or older than 3 Ma, given the inference that volcanism in the Sunda back-arc basin ceased about 3 Ma (Honthaas et al., 1998), however, some of the Banda arc seamounts (i.e. Banda Api, Serua, Nila, and Teon) are reported in the GVP, and erupted in recent times (within the last ~120 years). Other seamounts are found along this arc and include a stage 3 (New-02400)

and a stage 4 (New-02393) seamount. Although we lack geological information from these two volcanoes, their tectonic setting and proximity to other active seamounts may suggest that they were active in relatively recent times and may still present a potential threat for the region in case of eruption.

5.2 ~~Potential~~ Benefit of multibeam high-resolution image analysis

As part of the seamount characterisation, and where multibeam high-resolution (90-m/pixel) bathymetry data were available, we searched for morphological features on and around seamounts that may give us clues about past hazards (examples reported in Figure 7). Note that this information is reported here for discussion purposes only, rather than for quantitative assessment of frequency and type of these past events because multibeam data only covers < 10% of the region of interest, which may bias the results.

We identified several debris avalanche deposits, landslide scars and slumps, explosive craters at depth, new potential seamounts, and deposits associated with submarine explosive volcanic activity. To understand the potential of such past hazards, and the impact they would have if they occurred nowadays, we highlight an example of a large landslide scar and associated deposit near Kawio Barat seamount, in the Celebes Sea, ~100 km south of Mindanao and 90 km north of Sangihe Island, Indonesia (Fig. 7b). We roughly estimated the debris avalanche volume from the topographic contours (through Esri®ArcMap™ 10.7.1), which resulted in a volume of ~14 km^3 of material; the deposit includes visible blocks (i.e. hummocks) up to ~500 m in diameter, which are typical of massive sector collapses (Violante et al., 2003; Idárraga-García and León, 2019; Carter et al., 2020). For comparison, the sector collapse of Mt Krakatau volcano, Indonesia, in 2018, was about 0.15 km^3, which produced a local tsunami with maximum run-up of up to 14 m, and caused over 430 fatalities and millions of USD damage (Paris et al., 2020 and references therein). The event considered here is likely two orders of magnitude larger than the Krakatau event, and although the associated potential tsunami hazard cannot be compared directly because of bathymetric differences at both sites, the size of this event in the Sangihe arc gives us an idea of the relative scale.

Slumps are generally considered less likely to produce significant tsunamis, however, in some instances they have been inferred as the main cause of devastating tsunamis, such as the 1998 Papua New Guinea event (Okal and Synolakis, 2003; Brune et al., 2010). Subaqueous slumps appear as transverse ridges with steep toes and block of various sizes, as have been observed from bathymetric surveys around Hawaii (Moore et al., 1989), and ~~differently from~~in contrast to debris avalanches, they are not associated with any amphitheatre-like detachment area. An example is shown in Fig. 7a, where an area of over 100 km^2 of slumped material is highlighted, just north of seamount New-00919.

Explosive craters provide evidence of volcanic hazards; in Figure 7c we report an example from seamount KW-21797, ~300 km east-southeast of Taiwan and ~400 km northeast of Luzon, which is a composite and stage 2 seamount, and has a prominent topographic relief with a circular depression at the base of its NW side. This topographic feature is at a water depth of about 4,600 m, has a crater diameter of approximately 1.5 km and is around 150 m deep. We interpret this structure as a possible explosive crater because of its relatively large crater diameter and rather regular circular shape, which may have been formed by an individual explosive event. To the west of this structure, we identified an apron-like morphology extending westward for about 4 km, which is likely the volcanic deposit associated with this explosive structure mantling its flank. Though, we cannot rule out the possibility that this structure and associated deposit may be related to effusive activity forming a westward lava flow. Evidence of explosive volcanism at water depths ≥ 1000 m has been reported in literature, both along

volcanic arcs (Murch et al., 2019b), mid-ocean ridges (Sohn et al., 2008), and hotspots (Schipper et al., 2010). Additionally, the potential occurrence of explosive deep-sea volcanic eruptions has been proved through analogue experiments (Dürig et al., 2020; Newland et al., 2022; Head and Wilson, 2003).

In the same area of seamount KW-21797, we identified other possible seamounts (Fig. 7d) that are not reported in any official dataset. They are individual composite edifices or chains of composite edifices (at least 3 chains can be recognised, all extending along W-E trends). These potential seamounts vary in height from < 500 m to ~1500 m, and their summit reaches water depths of ~5,500 to ~4,000 m b.s.l. Although all these seamounts have their summit in deep waters, some of them are higher than 1,000 m (stage 2). We do not include them in SEATANI as we cannot be sure that they are volcanic, but they may be worth further investigation.
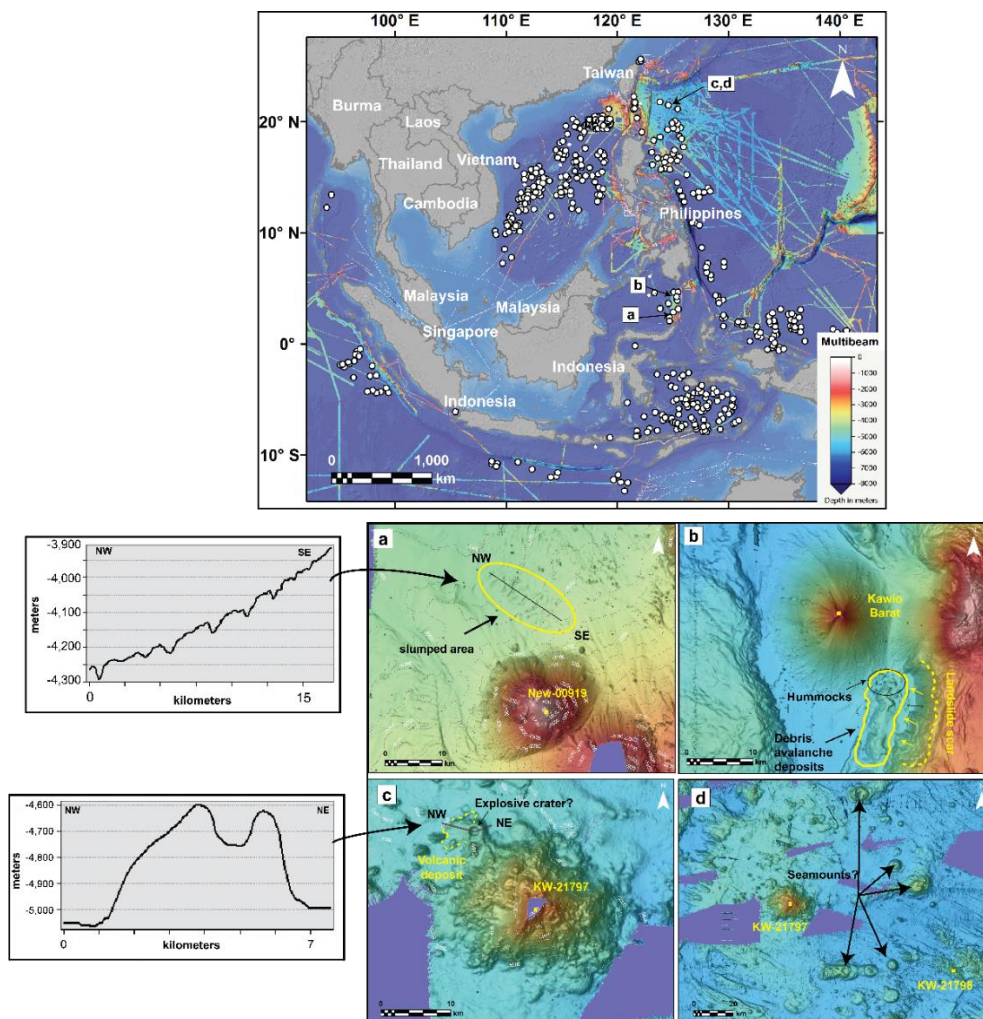
Figure 7. Map of the study region with multibeam data coverage (top panel), and relevant hazard features at some of the seamounts investigated, where multibeam data were available (bottom panels, a to d). Two bathymetric profiles for box a) and c) are also shown.

5.3 ~~Potential areas of interest~~Countries with high hazard/exposure potential

Our seamount characterisation and exposure potential analyses highlights areas potentially more exposed to hazards in case of submarine eruption in and around SEA. Taiwan seems to be the candidate that requires more attention. It ranks high for both exposure analysis types conducted here. It has the highest number of people exposed, with two stage 4 and one stage 3 seamount (the most hazardous types) just 30-60 km northeast of the

highly populated Taipei District (>9 M people). A submarine eruption at such distances may affect the nearby Taiwan through tephra falls and tsunamis. Subaqueous landslides, PDCs, or lava flows can damage the dense submarine cables array both north and south of Taiwan. Both volcanic and tsunami hazards can affect local ship traffic, which seems to be the densest in the whole region, with key connection between Taiwan and the rest of the region through eight major ports.

Besides Taiwan, if we consider the exposure by number and type of seamount by country (Fig. 5), Indonesia, Philippines and Vietnam are potentially threatened too. For Indonesia, the well-known Krakatau volcano is a hazard for population (~8 M people) and ship traffic, being a key passage to the South China Sea from the southern Indian Ocean. Eastern Indonesia (Sulawesi, Maluku and Lesser Sunda Island) is mostly exposed to stage 4, stage 3, and stage 2 seamounts. The Philippines is highly exposed as well, with the maximum exposures in the north (submarine cables, coasts), west (ship traffic) and south (coasts). Vietnam is characterised by high ship traffic density, with major commercial areas including the Mekong delta and Da Nang port. The Vietnam EEZ encloses a seamount that erupted in historical time, Ile des Cendres, 1923 (~115 km off the southeast coasts of Vietnam; Lat: 10.16°, Lon: 109.01). The eruption formed two islands (eroded soon after the eruption and now completely underwater) and at least another submarine cone (Global Volcanism Program, 2013). There is not much information about the eruption, but it was thought to be VEI= 2, and a local tsunami along the SE coasts of mainland Vietnam was also reported (Vu, 2008; Dai Dien, 2010). To our knowledge, there is no detailed study of the Ile Des Cendres complex, despite it representing the latest episode of submarine volcanism in the region and having a distributed nature (formation of several vents), which increases the area from which a potential eruption may occur, hence the hazard.

In areas of low seamount density and apparent lower hazard - for example the Indian EEZ (Andaman Sea, between Sumatra and Burma), which contains just two seamounts, both stage 4 - tsunami can potentially affect wider areas, such as the coasts of Thailand, Malaysia, Burma, Indonesia (Sumatra), India and, depending on the magnitude of the event, the coast of Singapore through the Malacca Strait. One of these seamounts is Barren Island, which shows past evidence of sector collapse (Chandrasekharam et al., 2009). Given the tectonic setting of these two volcanoes (submarine continuation of the Indonesian volcanic arc), we may expect the presence of other seamounts in this area not currently charted, hence potential increased hazard extent.

5.3.1 The geodynamic context for SEATANI seamounts

We noted that geology, absolute age, and eruption frequency/magnitude, were not taken into account for our hazard-exposure potential assessment, because of the lack of information for most of the seamounts in the region. Notwithstanding, in this section we discuss the geodynamic context of the SEATANI seamounts from a regional perspective, with a particular focus on the two regions that we found to host the highest number of stage 3 and 4, hence potentially more hazardous, seamounts: the South China Sea and the Banda Sea.

There are a number of seamounts (Fig. 6) in proximity to the Indonesian and Philippines trenches that show zero to very low weighted density, and this reflects their relatively low hazard potential. Seamounts in these particular tectonic settings are likely millions of years old and no longer active, being at the end of their cycle and approaching a subduction zone (Staudigel and Clague, 2010). It is likely that also some seamounts in the high weighted density regions of the South China Sea and Banda Sea may have been extinct for millions of years, however, these areas represent different tectonic settings, and must be discussed separately.

The South China Sea is the result of a multiphase continental rifting and breakup from the Eocene to the Miocene (e.g. Franke, 2013). Many studies provide evidence for extensive intraplate volcanism in the South China Sea following the end of the continental rifting (e.g. Xia et al., 2018; Gao et al., 2019; Zhao et al., 2020), with abundance of Late Cenozoic OIB-type basalts, inferred to be linked to a mantle plume (Yang et al., 2019). A more recent study identified widespread and partially still ongoing hydrothermal activity in the northern South China Sea, thought to be associated with magma intrusion (Zhao et al., 2021). On the southwestern edge of the South China Sea, east of southern Vietnam, there is a submarine volcano that erupted in historical times, Ile des Cendres, 1923. The volcano is located in proximity to a major regional fault, the East Vietnam Fault (Hall and Morley, 2004; Li et al., 2013) (Fig. 1); other major faults exist in the region (Mae Ping Fault and Three Pagodas Fault (Hall and Morley, 2004; Li et al., 2013), Fig. 1), and others may not be mapped, together with volcanoes in their proximity. Therefore, despite the intraplate setting, volcanism in the South China Sea may still play a role for future hazardous scenarios for the region.

The Banda Sea, on the other hand, results from more complex dynamics. This area was formed by the initial collision between the Australian and the Banda arc (which was already active from ~12 Ma, (Yang et al., 2021), and subsequent slab rollback, which created the extensional Banda Sea backarc basin (Wei et al., 2023). Therefore, seamounts in this area belong to at least two different formation mechanisms, arc volcanism and backarc extensional volcanism. If we consider the seamount growth stage for this area (Fig. 3b), we notice that that majority of seamounts along the Banda arc are stage 3 and 4, while the seamounts in the central portion of the Banda Sea basin are stage 2. Most of these stage 2 seamounts are likely as old or older than 3 Ma, given the inference that volcanism in the Sunda backarc basin ceased about 3 Ma (Honthaas et al., 1998), however, some of the Sunda arc seamounts (i.e. Banda Api, Serua, Nila, and Teon) are reported in the GVP, and erupted in recent times (within the last ~120 years). Other seamounts are found along this arc and include a stage 3 (New 02400) and a stage 4 (New 02393) seamount. Although we lack geological information from these two volcanoes, their tectonic setting and proximity to other active seamounts may suggest that they were active in relatively recent times and may still present a potential threat for the region in case of eruption.

5.4 Limitations and future goals

A major limitation of this study is the fact that we characterise the hazard potential from seamounts solely based on morphological (morphotype) and structural information (i.e. water depths, heights), with the high likelihood of including volcanoes that might have been inactive for millions of years, in turn resulting in an overestimation of the hazard potential. Despite this, the present study is relevant because it provides the elements to narrow down the research for future hazard studies from submarine volcanic activity in and around SEA.

The choice of the main seamount dataset used for our analysis, that from Gevorgian et al. (2023), was justified by at least two reasons: (1) it is the most up-to-date seamount dataset in terms of data quality of the Vertical Gravity Gradient (data noise reduction of 40% from previous VGG datasets; Gevorgian et al., 2023); and (2) it only focuses on volcanic seamounts, not including small volcanic features such as knolls, which are negligible in terms of volcanic hazards, and other non-volcanic large features. Even though their method excludes potential seamounts from within continental margins, potentially biasing our results toward lower hazard potential from areas such as the Sunda Shelf, we consider it a first approach to be improved upon with higher resolution data. The use of other global seamount datasets (Cañón-Tapia, 2023, and references therein), which include a higher number of seamounts (e.g. 33,452 seamounts and 138,412 knolls; Yesson et al., 2011), may have the opposite

effect leading to an overestimation of the hazard potential. Future studies should work to integrate the multiple other seamount datasets, supported by higher resolution bathymetry datasets, when made available, which will also help to characterise the large number of unclassifiable seamounts (n= 171) from this study.

On a parallel note, here we focused on submarine volcanism and excluded large volcanic islands and coastal volcanoes, however, we acknowledge that similar hazards to those produced by seamounts can be generated by such volcanoes, and extensive work has been already carried out in SEA (Zorn et al., 2022, and references therein). Therefore, future work can take advantage of both approaches for a more comprehensive assessment for the region.

The lack of seamounts identified on the Sunda shelf using our method and datasets is a shortcoming of using the (Gevorgian et al., (2023) dataset that filters out seamounts near continental margins. The known submarine volcanoes of Ile des Cendres and Veteran, alongside terrestrial volcanoes not reported in this study (e.g. Ly Son group, Table S2), ~~The general lack of seamounts on the Sunda shelf is questionable. Ile des Cendres and Veteran, besides other volcanoes not reported in this study because not in line with the definition of seamount used here (e.g. Ly Son group, Table S2),~~ are in close proximity with a major regional fault, the East Vietnam Fault. Since this fault extends across the central-eastern portion of the Sunda shelf (all the way south to Borneo inland) (Li et al., 2013), it would not be surprising to have other volcanoes along or near to this fault zone. Other major faults mapped on the Sunda shelf include the Wang Chao (Hall and Morley, 2004) and Three Pagogas faults (Li et al., 2013), but no seamount is known to exist around these areas. The number and type of seamounts potentially not mapped and not considered for this study, may bias our results, particularly with regards to the KDE assessment. Potentially, the threat to countries not currently considered exposed, e.g. Singapore, is much greater than currently appreciated, because of the lack of continental shelf mapped seamounts. However, once again, we emphasize that here we did not produce any volcanic hazard maps for the region, but rather conducted a ~~simple but necessary~~preliminary assessment of hazard and exposure potential, highlighting seamounts and areas of interest that can be the focus for more-in-depth studies.

When it comes to explosive versus effusive behaviour of a given volcano, hence the type of hazards it can produce, magma composition is a key aspect to consider. In subaerial environments, more silicic magmas are generally more explosive than basaltic magmas. However, in subaqueous environments the interaction between external water and magma is often consider the leading trigger of the explosivity of that particular volcano (e.g. Verolino et al., 2018, 2019). Many pioneer studies on the topic showed that this explosive interaction is more likely to occur with basaltic magmas (e.g. Wohletz, 1983, 1986; Büttner and Zimanowski, 1998), nevertheless, it also occurs with more silicic compositions (e.g. Austin-Erickson et al., 2008; Dürig et al., 2020). Magma composition was not accounted for in our assessment of hazard-exposure potential for two main reasons: 1) Only GVP seamounts have known composition (despite it could be assumed for some of the seamounts based on their tectonic setting); And 2) explosivity in subaqueous settings have been observed/inferred across all compositional domains, hence producing similar hazards regardless of composition. However, one difference is the production of pumice rafts in silicic eruptions (e.g. Havre, 2012; Fukutoku-Oka-no-Ba, 2021; Carey et al., 2014; Maeno et al., 2022), which is not expected for basaltic eruptions. Magma composition, eruption dynamics, and environmental factors that affect hazard extent, distribution and intensity, such as wind conditions or bathymetry, should be accounted for in future quantitative hazard studies for the region once more information is made available.

Two main issues about the study of seamounts globally and regionally are that 1) the detection from space is limited within continental margins, and 2) the currently available bathymetry resolution is not enough to allow a comprehensive morphological characterisation of seamounts. As a result, we end up with large areas without seamounts (e.g. Sunda shelf), and many unclassified seamounts (n= 171). ~~The general lack of seamounts on the Sunda shelf is questionable. Ile des Cendres and Veteran, besides other volcanoes not reported in this study because not in line with the definition of seamount used here (e.g. Ly Son group, Table S2), are in close proximity with a major regional fault, the East Vietnam Fault. Since this fault extends across the central-eastern portion of the Sunda shelf (all the way south to Borneo inland) (Li et al., 2013), it would not be surprising to have other volcanoes along or near to this fault zone. Other major faults mapped on the Sunda shelf include the Wang Chao (Hall and Morley, 2004) and Three Pagodas faults (Li et al., 2013), but no seamount is known to exist around these areas. The number and type of seamounts potentially not mapped and not considered for this study, may bias our results, particularly with regards to the KDE assessment. Potentially, the threat to countries not currently considered exposed, e.g. Singapore, is much greater than currently appreciated, because of the lack of continental shelf mapped seamounts. However, once again, we emphasize that here we did not produce any volcanic hazard maps for the region, but rather conducted a simple but necessary assessment of hazard and exposure potential, highlighting seamounts and areas of interest that can be the focus for more in-depth studies.~~

For the quantitative exposure analysis, we used a 100 km radius around each seamount to indicate areas that may be impacted by volcanic activity. However, concentric radii, despite used in previous hazard studies, are not a necessarily good approximation of how volcanic hazards behave (Jenkins et al., 2022): some hazards may affect areas smaller (e.g. lava flows, PDCs) or larger than the 100 km radius (e.g. tephra fall, pumice rafts).

Another limitation regards the exact location of submarine communication cables and how many people rely on this technology. The communication companies provide station to station information, which means that the exact path of each cable may not be as reported, and this probably partially affects our exposure results. Additionally, all countries in our study region depend on submarine cables for internet use, which translates into over 600 million people in the region, however, the cable length analysed here does not give a direct information on the potential impact from a submarine volcanic eruption, which would be provided, for example, by the exact number of people that rely on specific cables per country. Despite this limitation, the direct relationship of seamount and cable density in some areas (northern South China Sea, Luzon Strait, East China Sea) is rather obvious (Fig. S2) and should be accounted for with regards to future cable installations in the region.

The above limitations can be overcome in different ways. One is to improve our collaborative effort with private and government agencies, which may have seismic and bathymetry data that may improve our understanding of volcanic hazards from submarine volcanoes in the region. Another is to improve the existing bathymetry datasets, by combining direct bathymetric information from Gebco and from local nautical charts (Felix et al., 2022); this will help with a better regional seamount characterisation, hazard assessment, and eventually hazard modelling and impact analysis at key locations. A third possibility is to use new satellite altimetry data of the sea surface, which will be made available from NASA in 2024 through the SWOT (Surface Water and Ocean Topography) mission, which was launched in December 2022. These new data will provide unprecedented resolutions of the sea surface, which in turn will be used to estimate location of smaller seamount than those currently detectable from satellite-derived methods, at a global scale. These data could be combined with the bathymetry data for more

comprehensive analyses of hazard. Lastly, the results reported in this work, in addition to new data, will provide an evidence base for more focused investigations to be conducted at potentially high threatening seamounts (including sampling through Remotely Operated Vehicles, and later laboratory analysis for a complete characterisation). This will serve countries across the region to become more prepared and resilient against submarine volcanic hazards.

6 Conclusions

Seamounts are an understudied and potentially silent and unseen threat for human populations and infrastructure. Despite the global identification of about 35,000 seamounts (Gevorgian et al., 2023), only a few of them are thoroughly studied and monitored (e.g. Deardorff et al., 2011; Caress et al., 2012; Carey et al., 2014; Berthod et al., 2021). We conducted a seamount characterisation and associated hazard-exposure potential assessment on a regional scale for SEA and surrounding areas, through the SEATANI dataset, which provides the basis for more focused investigations of hazards for the region in the future at key locations. Our results show that composite and stage 2 seamounts are the most abundant in the region, however, stage 3 and stage 4 seamounts (simple, composite and calderas) are the most important for hazard potential and numbers of people, lengths of cable and density of shipping exposed. Taiwan has the highest total exposure potential (across all exposure types) within 100 km of volcanic seamounts, followed by Indonesia, Philippines and Vietnam. The hazard-weighted seamount density assessment highlights two main areas of interest: the northern South China Sea and the Banda Sea. Any volcanic and related hazards (e.g. tsunamis), if generated in these areas, will potentially affect the coasts of Southern Taiwan, northern and southern Philippines, Vietnam and eastern Indonesia.

This work represents the first step towards understanding the threat that submarine volcanoes pose to populations and infrastructure in and around SEA. The integration of new bathymetry, seismic and satellite-derived altimetry data (i.e. SWOT mission) will shed more light on the potential of these volcanoes and enhance awareness, preparedness and resilience for the countries surrounding these waters.

Data availability

Data are available in the supplementary material files and in the public data repository of NTU (https://researchdata.ntu.edu.sg/privateurl.xhtml?token=820ea7c9-4ff4-48f8-8e8b-98cd4ffe01f8)

References

Austin-Erickson, A., Büttner, R., Dellino, P., Ort, M. H., and Zimanowski, B.: Phreatomagmatic explosions of rhyolitic magma: Experimental and field evidence, J. Geophys. Res., 113, B11201, https://doi.org/10.1029/2008JB005731, 2008.

Berthod, C., Médard, E., Bachèlery, P., Gurioli, L., Di Muro, A., Peltier, A., Komorowski, J.-C., Benbakkar, M., Devidal, J.-L., Langlade, J., Besson, P., Boudon, G., Rose-Koga, E., Deplus, C., Le Friant, A., Bickert, M., Nowak, S., Thinon, I., Burckel, P., Hidalgo, S., Kaliwoda, M., Jorry, S. J., Fouquet, Y., and Feuillet, N.: The 2018-ongoing Mayotte submarine eruption: Magma migration imaged by petrological monitoring, Earth and Planetary Science Letters, 571, 117085, https://doi.org/10.1016/j.epsl.2021.117085, 2021.

Brown, S. K., Sparks, R. S. J., and Jenkins, S. F.: Global distribution of volcanic threat, in: Global Volcanic Hazards and Risk, edited by: Loughlin, S. C., Sparks, S., Brown, S. K., Jenkins, S. F., and Vye-Brown, C., Cambridge University Press, 359–370, https://doi.org/10.1017/CBO9781316276273.025, 2015.

711 Brune, S., Babeyko, A. Y., Gaedicke, C., and Ladage, S.: Hazard assessment of underwater landslide-generated
712 tsunamis: a case study in the Padang region, Indonesia, Nat Hazards, 53, 205–218,
713 https://doi.org/10.1007/s11069-009-9424-x, 2010.

714 Büttner, R. and Zimanowski, B.: Physics of thermohydraulic explosions, Phys. Rev. E, 57, 5726–5729,
715 https://doi.org/10.1103/PhysRevE.57.5726, 1998.

716 Cañón-Tapia, E.: Seamount chains and hotspot tracks: Superficially similar, deeply different, Geoscience
717 Frontiers, 14, 101659, https://doi.org/10.1016/j.gsf.2023.101659, 2023.

718 Caress, D. W., Clague, D. A., Paduan, J. B., Martin, J. F., Dreyer, B. M., Chadwick, W. W., Denny, A., and Kelley, D.
719 S.: Repeat bathymetric surveys at 1-metre resolution of lava flows erupted at Axial Seamount in April 2011,
720 Nature Geosci, 5, 483–488, https://doi.org/10.1038/ngeo1496, 2012.

721 Carey, R. J., Wysoczanski, R., Wunderman, R., and Jutzeler, M.: Discovery of the Largest Historic Silicic Submarine
722 Eruption, Eos, Transactions American Geophysical Union, 95, 157–159, https://doi.org/10.1002/2014EO190001,
723 2014.

724 Carter, G. D. O., Cooper, R., Gafeira, J., Howe, J. A., and Long, D.: Morphology of small-scale submarine mass
725 movement events across the northwest United Kingdom, Geomorphology, 365, 107282,
726 https://doi.org/10.1016/j.geomorph.2020.107282, 2020.

727 Cas, R. A. F.: Submarine volcanism; eruption styles, products, and relevance to understanding the host-rock
728 successions to volcanic-hosted massive sulfide deposits, Economic Geology, 87, 511–541,
729 https://doi.org/10.2113/gsecongeo.87.3.511, 1992.

730 Chadwick, W. W., Cashman, K. V., Embley, R. W., Matsumoto, H., Dziak, R. P., de Ronde, C. E. J., Lau, T. K.,
731 Deardorff, N. D., and Merle, S. G.: Direct video and hydrophone observations of submarine explosive eruptions
732 at NW Rota-1 volcano, Mariana arc: SUBMARINE EXPLOSIVE ERUPTIONS AT NW ROTA-1, J. Geophys. Res., 113,
733 https://doi.org/10.1029/2007JB005215, 2008.

734 Chandrasekharam, D., Santo, A. P., Capaccioni, B., Vaselli, O., Alam, M. A., Manetti, P., and Tassi, F.:
735 Volcanological and petrological evolution of Barren Island (Andaman Sea, Indian Ocean), Journal of Asian Earth
736 Sciences, 35, 469–487, https://doi.org/10.1016/j.jseaes.2009.02.010, 2009.

737 Clague, D. A., Holcomb, R. T., Sinton, J. M., Detrick, R. S., and Torresan, M. E.: Pliocene and Pleistocene alkalic
738 flood basalts on the seafloor north of the Hawaiian islands, Earth and Planetary Science Letters, 98, 175–191,
739 https://doi.org/10.1016/0012-821X(90)90058-6, 1990.

740 Clague, D. A., Paduan, J. B., Caress, D. W., Thomas, H., Chadwick Jr., W. W., and Merle, S. G.: Volcanic morphology
741 of West Mata Volcano, NE Lau Basin, based on high-resolution bathymetry and depth changes, Geochemistry,
742 Geophysics, Geosystems, 12, https://doi.org/10.1029/2011GC003791, 2011.

743 Clague, D. A., Dreyer, B. M., Paduan, J. B., Martin, J. F., Chadwick, W. W., Caress, D. W., Portner, R. A., Guilderson,
744 T. P., McGann, M. L., Thomas, H., Butterfield, D. A., and Embley, R. W.: Geologic history of the summit of Axial
745 Seamount, Juan de Fuca Ridge, Geochemistry, Geophysics, Geosystems, 14, 4403–4443,
746 https://doi.org/10.1002/ggge.20240, 2013.

747 Dai Dien, L.: Overview on tsunami risk evaluation and NPP project in Vietnam. 1st Kawashiwazaki International
748 Symposium on Seismic Safety of Nuclear Installations, 24–26 November 2010, NIIT, Niigata, Japan
749 (http://www.nsr.go.jp/archive/jnes/ seismic-symposium10/presentationdata/3_sessionB/B-09.pdf)., 2010.

750 Deardorff, N. D., Cashman, K. V., and Chadwick, W. W.: Observations of eruptive plume dynamics and pyroclastic
751 deposits from submarine explosive eruptions at NW Rota-1, Mariana arc, Journal of Volcanology and
752 Geothermal Research, 202, 47–59, https://doi.org/10.1016/j.jvolgeores.2011.01.003, 2011.

753 Diekmann, B., Hofmann, J., Henrich, R., Fütterer, D. K., Röhl, U., and Wei, K.-Y.: Detrital sediment supply in the
754 southern Okinawa Trough and its relation to sea-level and Kuroshio dynamics during the late Quaternary, Marine
755 Geology, 255, 83–95, https://doi.org/10.1016/j.margeo.2008.08.001, 2008.

756 Dürig, T., White, J. D. L., Murch, A. P., Zimanowski, B., Büttner, R., Mele, D., Dellino, P., Carey, R. J., Schmidt, L.
757 S., and Spitznagel, N.: Deep-sea eruptions boosted by induced fuel–coolant explosions, Nat. Geosci., 13, 498–
758 503, https://doi.org/10.1038/s41561-020-0603-4, 2020.

759 Dziak, R. P., Bohnenstiehl, D. R., Baker, E. T., Matsumoto, H., Caplan-Auerbach, J., Embley, R. W., Merle, S. G.,
760 Walker, S. L., Lau, T.-K., and Chadwick Jr., W. W.: Long-term explosive degassing and debris flow activity at West
761 Mata   submarine   volcano,   Geophysical   Research   Letters,   42,   1480–1487,
762 https://doi.org/10.1002/2014GL062603, 2015.

763 Embley, R. W., Chadwick, W. W., Baker, E. T., Butterfield, D. A., Resing, J. A., de Ronde, C. E. J., Tunnicliffe, V.,
764 Lupton, J. E., Juniper, S. K., Rubin, K. H., Stern, R. J., Lebon, G. T., Nakamura, K., Merle, S. G., Hein, J. R., Wiens,
765 D. A., and Tamura, Y.: Long-term eruptive activity at a submarine arc volcano, Nature, 441, 494–497,
766 https://doi.org/10.1038/nature04762, 2006.

767 Fan, C., Xia, S., Zhao, F., Sun, J., Cao, J., Xu, H., and Wan, K.: New insights into the magmatism in the northern
768 margin of the South China Sea: Spatial features and volume of intraplate seamounts: INTRAPLATE SEAMOUNTS
769 IN THE SCS, Geochem. Geophys. Geosyst., 18, 2216–2239, https://doi.org/10.1002/2016GC006792, 2017.

770 Felix, R. P., Hubbard, J. A., Bradley, K. E., Lythgoe, K. H., Li, L., and Switzer, A. D.: Tsunami hazard in Lombok and
771 Bali, Indonesia, due to the Flores back-arc thrust, Nat. Hazards Earth Syst. Sci., 22, 1665–1682,
772 https://doi.org/10.5194/nhess-22-1665-2022, 2022.

773 Feuillet, N., Jorry, S., Crawford, W. C., Deplus, C., Thinon, I., Jacques, E., Saurel, J. M., Lemoine, A., Paquet, F.,
774 Satriano, C., Aiken, C., Foix, O., Kowalski, P., Laurent, A., Rinnert, E., Cathalot, C., Donval, J.-P., Guyader, V.,
775 Gaillot, A., Scalabrin, C., Moreira, M., Peltier, A., Beauducel, F., Grandin, R., Ballu, V., Daniel, R., Pelleau, P.,
776 Gomez, J., Besançon, S., Geli, L., Bernard, P., Bachelery, P., Fouquet, Y., Bertil, D., Lemarchand, A., and Van der
777 Woerd, J.: Birth of a large volcanic edifice offshore Mayotte via lithosphere-scale dyke intrusion, Nat. Geosci.,
778 14, 787–795, https://doi.org/10.1038/s41561-021-00809-x, 2021.

779 Franke, D.: Rifting, lithosphere breakup and volcanism: Comparison of magma-poor and volcanic rifted margins,
780 Marine and Petroleum Geology, 43, 63–87, https://doi.org/10.1016/j.marpetgeo.2012.11.003, 2013.

781 Gao, J., Bangs, N., Wu, S., Cai, G., Han, S., Ma, B., Wang, J., Xie, Y., Huang, W., Dong, D., and Wang, D.: Post-
782 seafloor spreading magmatism and associated magmatic hydrothermal systems in the Xisha uplift region,
783 northwestern South China Sea, Basin Res, 31, 688–708, https://doi.org/10.1111/bre.12338, 2019.

784 Gevorgian, J., Sandwell, D. T., Yu, Y., Kim, S., and Wessel, P.: Global Distribution and Morphology of Small
785 Seamounts, Earth and Space Science, 10, e2022EA002331, https://doi.org/10.1029/2022EA002331, 2023.

786 Global Volcanism Program: Global Volcanism Program, 2013 (19 June 2021). Venzke, E (ed.). Smithsonian
787 Institution. Downloaded 19 Jun 2021. https://volcano.si.edu/volcano.cfm?vn=275813, 2013.

788 Gusman, A. R., Roger, J., Noble, C., Wang, X., Power, W., and Burbidge, D.: The 2022 Hunga Tonga-Hunga Ha'apai
789 Volcano Air-Wave Generated Tsunami, Pure Appl. Geophys., 179, 3511–3525, https://doi.org/10.1007/s00024-
790 022-03154-1, 2022.

791 Hall, R. and Morley, C. K.: Sundaland basins, in: Geophysical Monograph Series, vol. 149, edited by: Clift, P.,
792 Kuhnt, W., Wang, P., and Hayes, D., American Geophysical Union, Washington, D. C., 55–85,
793 https://doi.org/10.1029/149GM04, 2004.

794 Hammond, S. R.: Relationships between lava types, seafloor morphology, and the occurrence of hydrothermal
795 venting in the ASHES Vent Field of Axial Volcano, Journal of Geophysical Research: Solid Earth, 95, 12875–12893,
796 https://doi.org/10.1029/JB095iB08p12875, 1990.

797 Hamzah, L., Puspito, N. T., and Imamura, F.: Tsunami Catalog and Zones in Indonesia., Journal of Natural Disaster
798 Science, 22, 25–43, https://doi.org/10.2328/jnds.22.25, 2000.

799 Hanebuth, T. J. J., Voris, H. K., Yokoyama, Y., Saito, Y., and Okuno, J.: Formation and fate of sedimentary
800 depocentres on Southeast Asia's Sunda Shelf over the past sea-level cycle and biogeographic implications, Earth-
801 Science Reviews, 104, 92–110, https://doi.org/10.1016/j.earscirev.2010.09.006, 2011.

802 Harders, R., Ranero, C. R., and Weinrebe, W.: Characterization of Submarine Landslide Complexes Offshore Costa
803 Rica: An Evolutionary Model Related to Seamount Subduction. In S. Krastel et al. (eds.), Submarine Mass
804 Movements and Their Consequences, Advances in Natural and Technological Hazards Research 37, DOI
805 10.1007/978-3-319-00972-8 34, © Springer International Publishing Switzerland 2014, 2014.

806 Head, J. W. and Wilson, L.: Deep submarine pyroclastic eruptions: theory and predicted landforms and deposits,
807 Journal of Volcanology and Geothermal Research, 121, 155–193, https://doi.org/10.1016/S0377-
808 0273(02)00425-0, 2003.

809 Hidayat, A., Marfai, M. A., and Hadmoko, D. S.: Eruption on Indonesia's volcanic islands: a review of potential
810 hazards, fatalities, and management, IOP Conf. Ser.: Earth Environ. Sci., 485, 012061,
811 https://doi.org/10.1088/1755-1315/485/1/012061, 2020.

812 Honthaas, C., Réhault, J.-P., Maury, R. C., Bellon, H., Hémond, C., Malod, J.-A., Cornée, J.-J., Villeneuve, M.,
813 Cotten, J., Burhanuddin, S., Guillou, H., and Arnaud, N.: A Neogene back-arc origin for the Banda Sea basins:
814 geochemical and geochronological constraints from the Banda ridges (East Indonesia), Tectonophysics, 298,
815 297–317, https://doi.org/10.1016/S0040-1951(98)00190-5, 1998.

816 Idárraga-García, J. and León, H.: Unraveling the Underwater Morphological Features of Roncador Bank,
817 Archipelago of San Andres, Providencia and Santa Catalina (Colombian Caribbean), Front. Mar. Sci., 6, 77,
818 https://doi.org/10.3389/fmars.2019.00077, 2019.

819 Jenkins, S. F., Biass, S., Williams, G. T., Hayes, J. L., Tennant, E., Yang, Q., Burgos, V., Meredith, E. S., Lerner, G.
820 A., Syarifuddin, M., and Verolino, A.: Evaluating and ranking Southeast Asia's exposure to explosive volcanic
821 hazards, Nat. Hazards Earth Syst. Sci., 22, 1233–1265, https://doi.org/10.5194/nhess-22-1233-2022, 2022.

822 Jutzeler, M., Marsh, R., Carey, R. J., White, J. D. L., Talling, P. J., and Karlstrom, L.: On the fate of pumice rafts
823 formed during the 2012 Havre submarine eruption, Nat Commun, 5, 3660,
824 https://doi.org/10.1038/ncomms4660, 2014.

825 Kim, S.-S. and Wessel, P.: New global seamount census from altimetry-derived gravity data: New global
826 seamount census, Geophysical Journal International, 186, 615–631, https://doi.org/10.1111/j.1365-
827 246X.2011.05076.x, 2011.

828 Li, L., Clift, P. D., and Nguyen, H. T.: The sedimentary, magmatic and tectonic evolution of the southwestern
829 South China Sea revealed by seismic stratigraphic analysis, Mar Geophys Res, 34, 341–365,
830 https://doi.org/10.1007/s11001-013-9171-y, 2013.

831 Moore, J. G., Clague, D. A., Holcomb, R. T., Lipman, P. W., Normark, W. R., and Torresan, M. E.: Prodigious
832 submarine landslides on the Hawaiian Ridge, Journal of Geophysical Research: Solid Earth, 94, 17465–17484,
833 https://doi.org/10.1029/JB094iB12p17465, 1989.

834 Murch, A. P., White, J. D. L., and Carey, R. J.: Characteristics and Deposit Stratigraphy of Submarine-Erupted
835 Silicic Ash, Havre Volcano, Kermadec Arc, New Zealand, Front. Earth Sci., 7, 1,
836 https://doi.org/10.3389/feart.2019.00001, 2019a.

837 Murch, A. P., White, J. D. L., and Carey, R. J.: Unusual fluidal behavior of a silicic magma during fragmentation in
838 a deep subaqueous eruption, Havre volcano, southwestern Pacific Ocean, Geology, 47, 487–490,
839 https://doi.org/10.1130/G45657.1, 2019b.

840 Murch, A. P., Portner, R. A., Rubin, K. H., and Clague, D. A.: Deep-subaqueous implosive volcanism at West Mata
841 seamount, Tonga, Earth and Planetary Science Letters, 578, 117328,
842 https://doi.org/10.1016/j.epsl.2021.117328, 2022.

843 Mutaqin, B. W., Lavigne, F., Hadmoko, D. S., and Ngalawani, M. N.: Volcanic Eruption-Induced Tsunami in
844 Indonesia: A Review, IOP Conf. Ser.: Earth Environ. Sci., 256, 012023, https://doi.org/10.1088/1755-
845 1315/256/1/012023, 2019.

846 NCEI/WDS: National Geophysical Data Center / World Data Service: NCEI/WDS Global Historical Tsunami
847 Database. NOAA National Centers for Environmental Information. doi:10.7289/V5PN93H7, n.d.

848 Newland, E. L., Mingotti, N., and Woods, A. W.: Dynamics of deep-submarine volcanic eruptions, Sci Rep, 12,
849 3276, https://doi.org/10.1038/s41598-022-07351-9, 2022.

850 Ohno, Y., Iguchi, A., Ijima, M., Yasumoto, K., and Suzuki, A.: Coastal ecological impacts from pumice rafts, Sci
851 Rep, 12, 11187, https://doi.org/10.1038/s41598-022-14614-y, 2022.

852 Okal, E. A. and Synolakis, C. E.: Field survey and numerical simulations: a theoretical comparison of tsunamis
853 from dislocations and landslides. Pure Appl Geophys 160:2177–2188, 2003.

854 Omira, R., Ramalho, I., Terrinha, P., Baptista, M. A., Batista, L., and Zitellini, N.: Deep-water seamounts, a
855 potential source of tsunami generated by landslides? The Hirondelle Seamount, NE Atlantic, Marine Geology,
856 379, 267–280, https://doi.org/10.1016/j.margeo.2016.06.010, 2016.

857 Paris, A., Heinrich, P., Paris, R., and Abadie, S.: The December 22, 2018 Anak Krakatau, Indonesia, Landslide and
858 Tsunami: Preliminary Modeling Results, Pure Appl. Geophys., 177, 571–590, https://doi.org/10.1007/s00024-
859 019-02394-y, 2020.

860 Paris, R., Switzer, A. D., Belousova, M., Belousov, A., Ontowirjo, B., Whelley, P. L., and Ulvrova, M.: Volcanic
861 tsunami: a review of source mechanisms, past events and hazards in Southeast Asia (Indonesia, Philippines,
862 Papua New Guinea), Nat Hazards, 70, 447–470, https://doi.org/10.1007/s11069-013-0822-8, 2014.

863 Reyes-Hardy, M.-P., Aguilera Barraza, F., Sepúlveda Birke, J. P., Esquivel Cáceres, A., and Inostroza Pizarro, M.:
864 GIS-based volcanic hazards, vulnerability and risks assessment of the Guallatiri Volcano, Arica y Parinacota
865 Region, Chile, Journal of South American Earth Sciences, 109, 103262,
866 https://doi.org/10.1016/j.jsames.2021.103262, 2021.

867 Ribo, M., Cronin, S., Stern, S., Park, S. H., Garvin, J., and Kula, T.: Morphological evolution of the Hunga Tonga–
868 Hunga Ha'apai submarine volcano after the explosive eruption (No. EGU23-17221). Copernicus Meetings., 2023.

869 Schipper, C. I., White, J. D. L., Houghton, B. F., Shimizu, N., and Stewart, R. B.: "Poseidic" explosive eruptions at
870 Loihi Seamount, Hawaii, Geology, 38, 291–294, https://doi.org/10.1130/G30351.1, 2010.

871 Schmidt, R. A. L. F., Schmincke, H. U., and Sigurdsson, H.: Seamounts and island building. Encyclopedia of
872 volcanoes, 383-402., 2000.

873 Schnur, S. R., Chadwick Jr., W. W., Embley, R. W., Ferrini, V. L., de Ronde, C. E. J., Cashman, K. V., Deardorff, N.
874 D., Merle, S. G., Dziak, R. P., Haxel, J. H., and Matsumoto, H.: A decade of volcanic construction and destruction
875 at the summit of NW Rota-1 seamount: 2004–2014, Journal of Geophysical Research: Solid Earth, 122, 1558–
876 1584, https://doi.org/10.1002/2016JB013742, 2017.

877 Self, S.: Krakatau revisited: The course of events and interpretation of the 1883 eruption, GeoJournal, 28,
878 https://doi.org/10.1007/BF00177223, 1992.

879 Sims, K., Reith, A., Bright, E., McKee, J., and Rose, A.: LandScan Global 2021 [Data set]. Oak Ridge National
880 Laboratory. https://doi.org/10.48690/1527702, 2022.

881 Small, C. and Naumann, T.: The global distribution of human population and recent volcanism, Environmental
882 Hazards, 3, 93–109, https://doi.org/10.3763/ehaz.2001.0309, 2001.

883 Sohn, R. A., Willis, C., Humphris, S., Shank, T. M., Singh, H., Edmonds, H. N., Kunz, C., Hedman, U., Helmke, E.,
884 Jakuba, M., Liljebladh, B., Linder, J., Murphy, C., Nakamura, K., Sato, T., Schlindwein, V., Stranne, C.,
885 Tausenfreund, M., Upchurch, L., Winsor, P., Jakobsson, M., and Soule, A.: Explosive volcanism on the ultraslow-
886 spreading Gakkel ridge, Arctic Ocean, Nature, 453, 1236–1238, https://doi.org/10.1038/nature07075, 2008.

887 Speidel, U.: The Hunga Tonga Hunga Ha'apai Eruption – A Postmortem: What happened to Tonga's Internet in
888 January 2022, and what lessons are there to be learned?, in: Proceedings of the 17th Asian Internet Engineering
889 Conference, AINTEC'22: The 17th Asian Internet Engineering Conference, Hiroshima Japan, 70–78,
890 https://doi.org/10.1145/3570748.3570759, 2022.

891 Staudigel, H. and Clague, D.: The Geological History of Deep-Sea Volcanoes: Biosphere, Hydrosphere, and
892 Lithosphere Interactions, Oceanog., 23, 58–71, https://doi.org/10.5670/oceanog.2010.62, 2010.

893 Staudigel, H., Koppers, A. A. P., Lavelle, W., Pitcher, T. J., and Shank, T. M.: Defining the Word "Seamount," 2010.

894 Taha, G., Loughman, R., Colarco, P. R., Zhu, T., Thomason, L. W., and Jaross, G.: Tracking the 2022 Hunga Tonga-
895 Hunga Ha'apai Aerosol Cloud in the Upper and Middle Stratosphere Using Space-Based Observations,
896 Geophysical Research Letters, 49, https://doi.org/10.1029/2022GL100091, 2022.

897 TeleGeography: Worldwide   submarine   cables.
898 https://services.arcgis.com/6DIQcwlPy8knb6sg/arcgis/rest/services/SubmarineCables/FeatureServer
899 (Downloaded on 11 June 2021), n.d.

900 The World Bank: The January 15, 2022 Hunga Tonga-Hunga Ha'apai eruption and tsunami, Tonga Global Rapid
901 Post   Disaster   Damage   Estimation   (Grade)   Report.
902 https://thedocs.worldbank.org/en/doc/b69af83e486aa652d4232276ad698c7b-0070062022/original/GRADE-
903 Report-Tonga-Volcanic-Eruption.pdf, 2022.

904 The   World   Bank   Group: Global   Shipping   Traffic   Density.
905 https://datacatalog.worldbank.org/search/dataset/0037580. Downloaded on 13 July 2021., n.d.

906 Verolino, A., White, J. D. L., and Brenna, M.: Eruption dynamics at Pahvant Butte volcano, Utah, western USA:
907 insights from ash-sheet dispersal, grain size, and geochemical data, Bull Volcanol, 80, 1–18,
908 https://doi.org/10.1007/s00445-018-1256-7, 2018.

909 Verolino, A., White, J. D. L., Dürig, T., and Cappuccio, F.: Black Point – Pyroclasts of a Surtseyan eruption show
910 no change during edifice growth to the surface from 100 m water depth, Journal of Volcanology and Geothermal
911 Research, 384, 85–102, https://doi.org/10.1016/j.jvolgeores.2019.07.013, 2019.

912 Verolino, A., Jenkins, S. F., Sieh, K., Herrin, J. S., Schonwalder-Angel, D., Sihavong, V., and Oh, J. H.: Assessing
913 volcanic hazard and exposure to lava flows at remote volcanic fields: a case study from the Bolaven Volcanic
914 Field, Laos, J Appl. Volcanol., 11, 6, https://doi.org/10.1186/s13617-022-00116-z, 2022a.

915 Verolino, A., White, J. D. L., Baxter, R. J. M., Schipper, C. I., and Thordarson, T.: Characteristics of Sub-Aerially
916 Emplaced Pyroclasts in the Surtsey Eruption Deposits: Implications for Diverse Surtseyan Eruptive Styles,
917 Geosciences, 12, 79, https://doi.org/10.3390/geosciences12020079, 2022b.

918 Violante, C., Budillon, F., Esposito, E., Porfido, S., and Vittori, E.: Submerged Hummocky Topographies And
919 Relations With Landslides. Northwestern Flank Of Ischia Is- Land, Southern Italy, 2003.

920 Vu,   T.   C.:   Earthquake   and   Tsunami   Scenarios   in   the   South   China   Sea
921 (www.ims.nus.edu.sg/Programs/ocean07/files/vu1.ppt), 2008.

922 Wang, Q., Guo, J., Wang, Z., Tahchi, E., Wang, X., Moran, B., and Zukerman, M.: Cost-Effective Path Planning for
923 Submarine Cable Network Extension, IEEE Access, 7, 61883–61895,
924 https://doi.org/10.1109/ACCESS.2019.2915125, 2019.

925 Wei, X., Luan, X., Meng, F., Lu, Y., He, H., Qiao, J., Yin, J., Wang, Y., and Xue, Y.: Deformation feature and tectonic
926 model of the Timor Trough: New interpretation of the evolution and mechanism of Banda arc-continent
927 collision, Tectonophysics, 862, 229958, https://doi.org/10.1016/j.tecto.2023.229958, 2023.

928 Wessel, P.: Seamount Characteristics. In: Pitcher T, Morato T, et al., editors. Seamounts: Ecology, Fisheries, &
929 Conservation. Fish and Aquatic Resources Series 12. Blackwell Publishing., p. 3-20., 2007.

930 Whelley, P. L., Newhall, C. G., and Bradley, K. E.: The frequency of explosive volcanic eruptions in Southeast Asia,
931 Bull Volcanol, 77, 1, https://doi.org/10.1007/s00445-014-0893-8, 2015.

932 Wohletz, K. H.: Mechanisms of hydrovolcanic pyroclast formation: Grain-size, scanning electron microscopy, and
933 experimental studies, 33, 1983.

934 Wohletz, K. H.: Explosive magma-water interactions: Thermodynamics, explosion mechanisms, and field studies,
935 Bull Volcanol, 48, 245–264, https://doi.org/10.1007/BF01081754, 1986.

936 Xia, S., Zhao, F., Zhao, D., Fan, C., Wu, S., Mi, L., Sun, J., Cao, J., and Wan, K.: Crustal plumbing system of post-rift
937 magmatism in the northern margin of South China Sea: New insights from integrated seismology,
938 Tectonophysics, 744, 227–238, https://doi.org/10.1016/j.tecto.2018.07.002, 2018.

939 Yang, F., Huang, X.-L., Xu, Y.-G., and He, P.-L.: Plume-ridge interaction in the South China Sea: Thermometric
940 evidence from Hole U1431E of IODP Expedition 349, Lithos, 324–325, 466–478,
941 https://doi.org/10.1016/j.lithos.2018.11.031, 2019.

942 Yang, X., Singh, S. C., and Deighton, I.: The Margin-Oblique Kumawa Strike-Slip Fault in the Banda Forearc, East
943 Indonesia: Structural Deformation, Tectonic Origin and Geohazard Implication, Tectonics, 40,
944 https://doi.org/10.1029/2020TC006567, 2021.

945 Yesson, C., Clark, M. R., Taylor, M. L., and Rogers, A. D.: The global distribution of seamounts based on 30 arc
946 seconds bathymetry data, Deep Sea Research Part I: Oceanographic Research Papers, 58, 442–453,
947 https://doi.org/10.1016/j.dsr.2011.02.004, 2011.

948 Zhao, F., Alves, T. M., Xia, S., Li, W., Wang, L., Mi, L., Wu, S., Cao, J., and Fan, C.: Along-strike segmentation of
949 the South China Sea margin imposed by inherited pre-rift basement structures, Earth and Planetary Science
950 Letters, 530, 115862, https://doi.org/10.1016/j.epsl.2019.115862, 2020.

951 Zhao, F., Berndt, C., Alves, T. M., Xia, S., Li, L., Mi, L., and Fan, C.: Widespread hydrothermal vents and associated
952 volcanism record prolonged Cenozoic magmatism in the South China Sea, GSA Bulletin, 133, 2645–2660,
953 https://doi.org/10.1130/B35897.1, 2021.

954 Zorn, E. U., Orynbaikyzy, A., Plank, S., Babeyko, A., Darmawan, H., Robbany, I. F., and Walter, T. R.: Identification
955 and ranking of subaerial volcanic tsunami hazard sources in Southeast Asia, Nat. Hazards Earth Syst. Sci., 22,
956 3083–3104, https://doi.org/10.5194/nhess-22-3083-2022, 2022.

957

963   **Author contribution**

964   AV: Paper conceptualisation and preparation, figures production, data elaboration, analysis,

965   and interpretation, editing; SFW: data elaboration, analysis, and interpretation; SJ: paper conceptualisation,

966   editing; FC: paper conceptualisation, editing; ADS: paper conceptualisation, editing.

967   **Competing Interests**

968   We declare no competing interests.